Master's Thesis
석사 학위논문

Communication Channel Modeling and Capacity Analysis of Controller Area Network (CAN)

Donghyuk Jang (장 동 혁 張 洞 赫)

Department of Information and Communication Engineering
정보통신융합공학전공

DGIST

2015

Master's Thesis
석사 학위논문

Communication Channel Modeling and Capacity Analysis of Controller Area Network (CAN)

Donghyuk Jang (장 동 혁 張 洞 赫)

Department of Information and Communication Engineering

정보통신융합공학전공

DGIST

2015

Communication Channel Modeling and Capacity Analysis of Controller Area Network (CAN)

Advisor : Professor Ji-Woong Choi

Co-advisor : Professor Hui-Sub Cho

By

Donghyuk Jang
Department of Information and Communication Engineering
DGIST

A thesis submitted to the faculty of DGIST in partial fulfillment of the requirements for the degree of Master of Science in the Department of Information and Communication Engineering. The study was conducted in accordance with Code of Research Ethics[1]

May. 15. 2015

Approved by

Professor Ji-Woong Choi (Signature)
(Advisor)

Professor Hui-Sub Cho (Signature)
(Co-Advisor)

[1] Declaration of Ethical Conduct in Research**:** we, as a graduate student of DGIST, hereby declare that we have not committed any acts that may damage the credibility of my research. These include, but are not limited to: falsification, thesis written by someone else, distortion of research findings or plagiarism. We affirm that my thesis contains honest conclusions based on my own careful research under the guidance of my thesis advisor.

Communication Channel Modeling and Capacity Analysis of Controller Area Network (CAN)

Donghyuk Jang

Accepted in partial fulfillment of the requirements for the degree of Master of Science

May. 15. 2015

Head of Committee _____(인)
Prof. Ji-Woong Choi

Committee Member _____(인)
Prof. Hui-Sub Cho

Committee Member _____(인)
Prof. Jae-Eun Jang

감사의 글

대구경북과학기술원에 입학한 지가 엊그제 같은데 어느덧 졸업을 앞두고 있습니다. 이 논문이 나오기까지 연구실에서 많은 고생을 하고 좌절을 겪기도 했지만, 그보다도 연구실 사람들에게 많은 정이 들었고, 많은 것을 배움으로써 받은 것, 좋았던 것이 더욱 더 많았습니다.

먼저, 부족한 저를 이끌어 주시고 믿고 기다려주신 교수님께 깊은 감사의 뜻을 전합니다. 입학할 때부터 부족한 점이 많았지만, 저를 믿고 끝까지 저를 성장시키기 위해 마음고생을 심하게 하시며 저를 이끌어 주셨습니다. 교수님 덕분에 사회에 나가기 전 많은 것들을 배우고, 경험하게 되었습니다. 진심으로 감사합니다 교수님.

연구실 사람들에게도 많은 도움을 받았습니다. 항상 저의 말을 잘 들어주시고 이끌어 주셨던 한준이 형, 랩실의 발전을 위해 진심 어린 충고를 아끼지 않으셨던 경수형, 부족한 저에게 있어 CAN 통신을 잘 가르쳐 줬던 성민이, 묵묵히 자신의 일을 열심히 하면서 저를 도와주려 했던 성호, 저의 말을 잘 따라주며 마음을 다잡으며 열심히 했던 석현이, 부족한 사수 밑에서 묵묵히 자신의 일을 열심히 하며 저를 도와줬던 은민이. 모두 감사합니다.

이 외에도 2년 동안 슬픈 일, 기쁜 일이 있을 때 함께 웃고 기뻐해 주었던 여러 동기들에게도 감사의 말을 전합니다.

그리고, 저를 항상 믿고 묵묵히 응원해 주시는 부모님과 저의 동생 민석이에게도 감사의 말을 전합니다. 저를 믿어준 만큼, 최선을 다해 은혜에 보답할 수 있는 자랑스러운 아들, 형이 되도록 노력하겠습니다. 감사합니다.

마지막으로, 다시 한번 랩실의 구성원 모두에게 감사의 말을 전하며, 저와 함께 했던 모든 이들의 앞날에는 밝은 미래가 있기를 기원합니다. 몇 년 후에도, 몇 십 년 후에도 인연이 지속되어 서로 이끌어 주며, 의지할 수 있는, 술 한 잔 기울이며 그땐 그랬었지 라며 추억을 회상 하며 회포를 나눌 수 있는, 그런 인연이 되길 간절히 기원합니다. 모두 감사합니다.

2015년 7월

장동혁 드림

201322024 장 동 혁. Donghyuk Jang. Communication Channel Modeling and Capacity Analysis of Controller Area Network (CAN). 2015. 43p. Advisors Prof. Ji-Woong Choi, Co-Advisors Prof. Hui-Sub Cho.

ABSTRACT

Controller area network (CAN) has been widely used for in-vehicle networks. The demand of data rate of in-vehicle network has risen sharply, while traditional CAN communication cannot support this demand of data rate with limited bandwidth around DC. To overcome the limitation, passband communication systems can be considered where wider bandwidth may be available. In order to use the passband, we need to understand and analyze the CAN communication channel. However, since real measurement of the channel response takes so much time and efforts, it will be convenient if channel modeling of CAN communication system is available. In this paper, we perform modeling of passband CAN communication systems by using a transmission matrix and a cascade of two port network methods. Instead of real measurement, we expect to reduce the time and efforts significantly to obtain a passband CAN communication channel response by using the channel modeling result. Using channel modeling result, we suggest the bridge tap length and bandwidth for suitable designing passband CAN system. Furthermore, using channel modeling and noise measurement results described in this paper, we perform capacity analysis of each channel state in order to know maximum throughput of the system.

Keywords: Controller area network (CAN), Channel modeling, AWG 24 twisted pair, Transmission matrix, Capacity analysis.

Contents

Ⅰ. INTRODUCTION

Controller area network (CAN) is multi-master communication which supports data rates of up to 1 Mbps, first introduced by Robert Bosch in 1986 [1]. Since the CAN communication systems have advantages of robustness to errors and efficiency of control signal inside the vehicles, the CAN communication has been widely adopted for in-vehicle networking [1]. As the demand of electronic components inside the car has been sharply grown in modern-day vehicles, high data rate of CAN communication is needed. CAN with flexible data-rate (CAN-FD) supplements CAN in applications that require a higher data-rate, but it has average data rate of 2.5 Mbps with existing CAN transceivers [2]. The FlexRay communication's bus is a deterministic, fault-tolerant and high-speed bus system developed in conjunction with automobile manufacturers and leading suppliers. The data rate of Flexray is about 10Mbps, but it is required higher cost and more wire for inside vehicle communication [4]. Besides, Flexray data rate 10Mbps is still not sufficient for vehicle entertainment data demand.

These technologies have limitation of data rate because they use only baseband for communication. Baseband has a limitation of bandwidth, so in order to overcome the limitation of bandwidth and data rate, passband communication systems can be employed, where passband channel characteristics needs to be first known. However, preceding research on passband CAN communication has been hardly tried yet. Thus, we need to investigate the channel response of passband CAN communication. Since measuring of channel condition for numerous scenarios and configurations requires a lot of time and efforts, we need CAN channel modeling in a systematic manner.

We use channel modeling method which is used *R,L,G,C* parameters and propagation constant to calculate transmission matrix. The transmission matrix is transformed into main line form or bridge tap form. Using the main line or the bridge tap transmission matrix and properties of cascaded two-port network, we can obtain transfer function of CAN system.

The channel modeling method which we describe in this paper is similarly applied in power line communication (PLC) and very high bit rate digital subscriber line (VDSL) applications. However, unlike CAN with PLC and VDSL system, CAN communication systems use a bus topology structure, where the bridge tap length and the main line length are limited below 1m and 33m, respectively [3]. Besides, PLC and VDSL system did not consider arbitrary Tx-Rx pair's channel condition because transmitter is positioned the first part of the PLC and VDSL system. Thus, the PLC and VDSL system is not necessary to analyze channel response at arbitrary Tx-Rx pair. In addition, the PLC and VDSL uses low frequency band up to 20-30MHz because PLC is exposed to poor environment and VDSL is exposed to crosstalk interference which makes significant attenuation at high frequency. Different from PLC and VDSL, CAN is not only exposed to small outer noise, but also exposed to small crosstalk between two ECUs. Thus, the CAN system can use higher frequency band than the PLC and VDSL.

In this paper, comparing to PLC and VDSL, we conduct channel modeling of CAN communication systems at arbitrary Tx-Rx pair, confirm it using simulation and experiment results at frequency band range from 0Hz to 100MHz. Based on this result, we suggested a range of bridge tap length and bandwidth for designing CAN communication systems. We also analyze the tendency of null generation in case of arbitrary Tx-Rx pair.

Using the simulation result, we obtain an impulse response of each channel in order to know which signal transmission path is dominant. Finally, we obtain a capacity of each channel condition in order to know maximum data rate of the system.

The outline of the paper is organized as follows: First, the structure of CAN communication systems is described in Section II. Passband CAN communication is described in Section III. Next, channel model is described in Section IV. The noise measurement is given in Section V. Not only the modeling results are verified through comparison with experiments, but also analysis of impulse response, capacity shown in Section VI. Finally, Section VII provides conclusions and describes future work.

II. CAN communication systems

The CAN communication systems consists of main line and multiple bridge taps which are called as electronic control units (ECU) inside the vehicle. Fig. 1 shows a basic structure of the CAN communication system. This structure called as bus structure which is supported multi-master communication. The advantage of bus structure is any ECU can communicate to other ECU. Besides, This structure can reduce wiring complexity and cost when designing a car system.

Traditional CAN bus and bridge taps use AWG 24 twisted pair for transmission since it has a characteristic of canceling out electromagnetic interference (EMI) from external sources. Each end of system attached 120 ohm resistor in order to prevent reflection wave [5].

Destructive interference is generated at the intersection between a main line and a bridge tap because signal reflection occurs at the bridge tap. This interference makes a null which causes high attenuation in a frequency domain. Thus, we have to compensate this null when we design communication systems. For this reason, knowing channel response is important to determine channel bandwidth and system parameters.

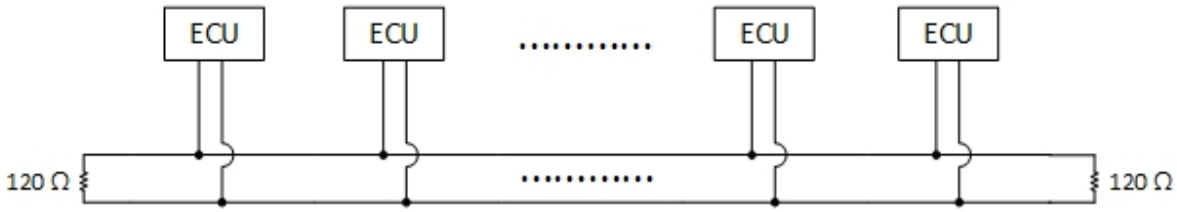

Fig.1. The CAN communication system structure

III. Passband CAN communication

The previous CAN system did not consider high data rate of CAN communication system because 1Mbps is enough to send control message to ECUs. However, the recent vehicle user wants to entertainment inside the vehicle. In entertainment of vehicle, for example, RSE (Real Seat Entertainment) or back and front camera, 1Mbps is not enough for multimedia. In addition, if the data rate of in-vehicle networking is increased, the complexity and cost of wiring in vehicle are significantly decreased. In order to be satisfied with these demand, at least 100Mbps data rate is needed.

Traditional CAN communication system only use baseband for transmission of signal. The baseband has a limitation of bandwidth which is caused limitation of data rate up to 1Mbps in traditional CAN system. CAN with flexible data-rate (CAN-FD) supports a higher data-rate, but it has average data rate of 2.5 Mbps with existing CAN transceivers. The CAN-FD uses baseband for data transmission, but it uses overclocking method to increase data rate. However, the overclocking method still has a limitation of data rate because CAN-FD data frame includes long period of arbitration and synchronization [2].

In order to overcome the limitation of bandwidth and data rate which is described in above, we suggest to passband CAN communication system for high data rate. If we use passband for CAN communication, we can use more bandwidth for transmission of signal. In addition, if we select modulation scheme which is optimized for CAN communication condition, we can increase data rate significantly.

Before applying passband system to CAN, we need to know channel response of the CAN communication system. According to transmission line theory, the insertion loss is increased as frequency is increased [6]. Because high insertion loss is occurred at high frequency, we consider the frequency range from 0Hz to 100MHz.

The traditional CAN signal uses baseband which have frequency range from DC level to 20MHz. To avoid interference between traditional CAN signal and passband CAN signal, we consider to use the frequency range from 20MHz to 100MHz for passband CAN communication in this paper.

IV. Channel model

4.1. End-to-end case

The procedure of obtaining CAN communication system's frequency response is as follows

1) Obtain AWG 24 twisted pair *R,L,G,C*.
2) Calculate propagation constant and characteristic impedance of AWG 24 twisted pair by using *R,L,G,C* parameters.
3) Set a transmission matrix of each line.
4) Get a total system transmission matrix by product of each line transmission matrix.
5) Get a frequency response using transmission matrix, source and load impedance of system.

AWG 24 twisted pair wire is replaced with *R,L,G,C* parameter which is called lumped circuit in the part of transmission line theory [6]. The European Telecommunications Standards Institute (ETSI) provides *R,L,G,C* model of AWG 24 twisted pair which is classified BT model #0 [7]. The *R,L,G,C* equations which represent AWG 24 twisted pair wire characteristics is expressed as

$$R(f) = \sqrt[4]{r_{0c}^4 + a_c f^2} \tag{1}$$

$$L(f) = \frac{l_0 + l_\infty \left(\frac{f}{fm}\right)^b}{1 + \left(\frac{f}{fm}\right)^b} \tag{2}$$

$$C(f) = c_\infty + c_0 f^{-c_e} \tag{3}$$

$$G(f) = g_0 f^{g_e} \tag{4}$$

where r_{0c} is the DC resistance due to copper and the separate skin effects for copper is accounted for by a_c. l_0 and l_∞ are the low and high-frequency inductances, respectively, and b is a parameter chosen to characterize the transition between low and high frequencies

in the measured inductance values for the series inductance. c_∞ is the contact capacitance and c_0 is a constant to fit the measurements for the shunt capacitance. Table I shows the detail value of each *R,L,G,C* component.

TABLE I
ETSI BT MODEL #0 – DETAIL VALUE OF THE PARAMETER

Parameters		Twisted pair type 2 (diameter 0.5 mm)
Resistance	r_{0c}	179.2 Ω/km
	a_c	0.0561
Inductance	l_0	674.6 µH/km
	l_∞	532.7 µH/km
	b	1.195
	f_m	664700 Hz
Capacitance	c_0	50 nF/km
	c_∞	0 nF/km
	c_e	0
Conductance	g_0	0 S/km

Next step is to obtain propagation constant and characteristic impedance of AWG 24 twisted pair by using *R,L,G,C* parameters. According to transmission line theory, the propagation constant is defined as [6]

$$\gamma(f) = \sqrt{\left(R(f) + j\omega L(f)\right)\left(G(f) + j\omega C(f)\right)} \tag{5}$$

and the characteristic impedance is defined as

$$Z_0 = \sqrt{\frac{\left(R(f) + j\omega L(f)\right)}{\left(G(f) + j\omega C(f)\right)}} \tag{6}$$

A twisted pair line which has a line length of l can be represented as a two-port network using a so-called ABCD model shown in Fig. 2 where the voltage V_1 and I_1 are voltage and

current at the left side port, whereas V_2 and I_2 are voltage and current at the right side port [6].

The transmission matrix is defined as

$$\begin{bmatrix} V_1 \\ I_1 \end{bmatrix} = \begin{bmatrix} A_1 & B_1 \\ C_1 & D_1 \end{bmatrix} \begin{bmatrix} V_2 \\ I_2 \end{bmatrix} \tag{7}$$

$$A_1 = \left.\frac{V_1}{V_2}\right|_{I_2=0}, B_1 = \left.\frac{V_1}{I_2}\right|_{V_2=0}, C_1 = \left.\frac{I_1}{V_2}\right|_{I_2=0}, D_1 = \left.\frac{I_1}{I_2}\right|_{V_2=0}. \tag{8}$$

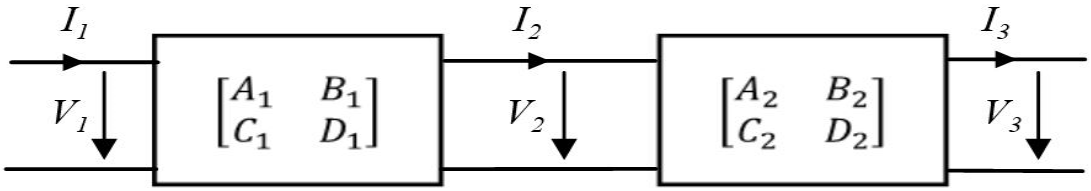

Fig. 2. Cascaded two port network with transmission parameters

According to transmission line theory, transmission line can be replaced as *R,L,G,C* parameters as shown in Fig. 3, where *L*, *R*, *C*, *G*, *dx* represent inductance per unit length, resistance per unit length, capacitance per unit length, admittance per unit length and line section of length, respectively. Using KVL and KCL, the telegrapher's equation is given by [6]

$$\frac{d^2V(x)}{dx^2} = \gamma^2 V(x) \tag{9}$$

$$\frac{d^2I(x)}{dx^2} = \gamma^2 I(x) \tag{10}$$

and the solution of telegrapher's equation is given by

$$V(x) = V_0^+ e^{-\gamma x} + V_0^- e^{\gamma x}, I(x) = \frac{V_0^+}{Z_0} e^{-\gamma x} - \frac{V_0^-}{Z_0} e^{\gamma x} \tag{11}$$

where x is the arbitrary distance of the line as shown in Fig. 4. $e^{-\gamma x}$ and $e^{\gamma x}$ are decay of incident wave and reflection wave, respectively. Z_0 is the characteristic impedance of the

line and γ is propagation constant.

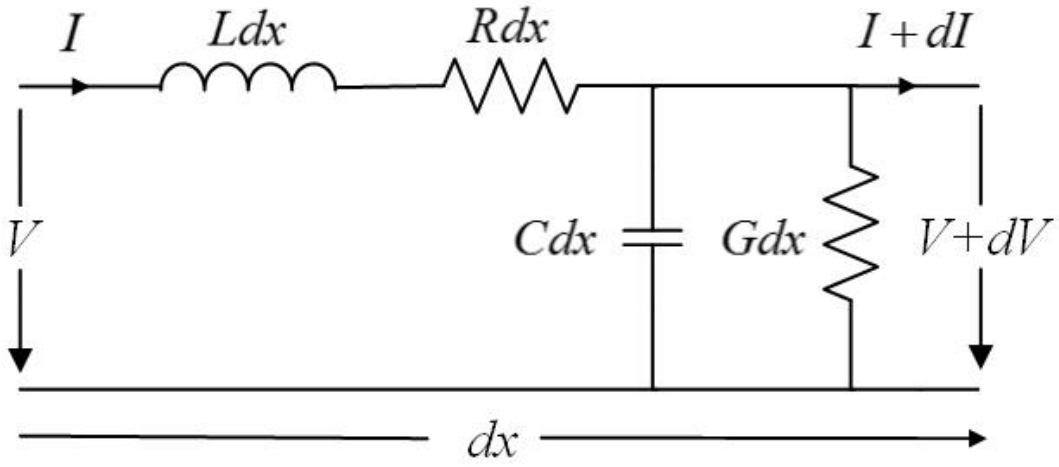

Fig. 3. Lumped circuit model of transmission line

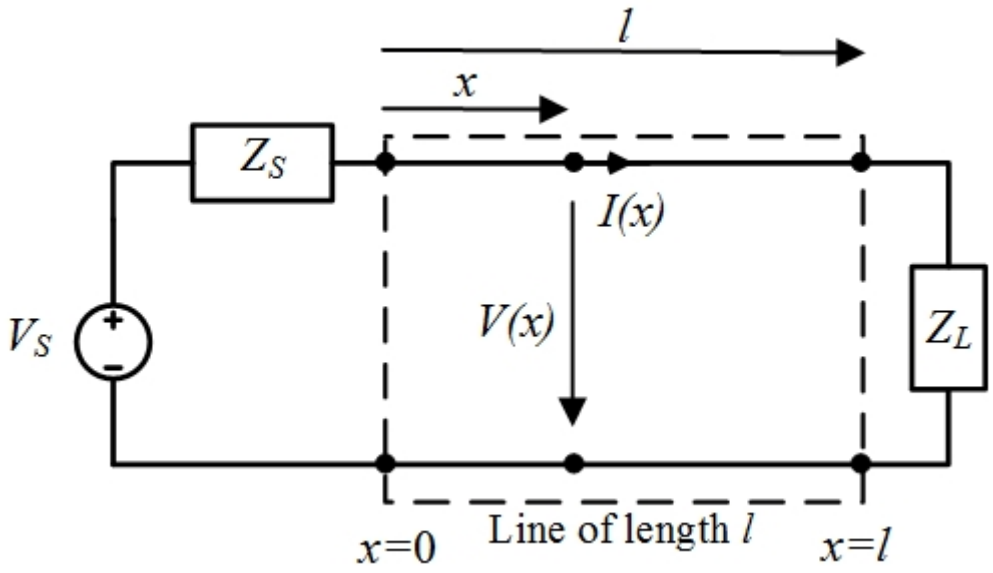

Fig. 4. Configuration of line section

The configuration of line section of length l is shown in Fig. 4 where l, Z_S, Z_L are the line of length, source generator internal impedance and load impedance, respectively. In case of $x = l$, V_0^+ and V_0^- can be represented as

$$V_0^+ = \frac{1}{2}\left(V(l) + Z_0 I(l)\right)e^{\gamma l}, V_0^- = \frac{1}{2}\left(V(l) - Z_0 I(l)\right)e^{-\gamma l}. \quad (12)$$

The initial position ($x = 0$) voltage can be expressed as

$$V(0) = V_0^+ + V_0^- = \frac{e^{\gamma l} + e^{-\gamma l}}{2} V(l) + Z_0 \frac{e^{\gamma l} - e^{-\gamma l}}{2} I(l). \tag{13}$$

Same procedure can be applied to $I(0)$ as

$$V(0) = \cosh(\gamma l) V(l) + Z_o \sinh(\gamma l) I(l) \tag{14}$$

$$I(0) = \frac{\sinh(\gamma l)}{Z_0} V(l) + \cosh(\gamma l) I(l). \tag{15}$$

Thus, the transmission matrix of the main line is given by

$$T = \begin{bmatrix} A & B \\ C & D \end{bmatrix} = \begin{bmatrix} \cosh(\gamma l) & Z_0 \sinh(\gamma l) \\ \dfrac{\sinh(\gamma l)}{Z_0} & \cosh(\gamma l) \end{bmatrix} \tag{16}$$

The configuration of bridge tap and main line is shown in the left side of Fig. 5. The bridge tap can be regarded as a two wire transmission line model, or can be replaced by *R,L,G,C* lumped circuit model which can be summarized into an impedance of line as in the right side of Fig. 5.

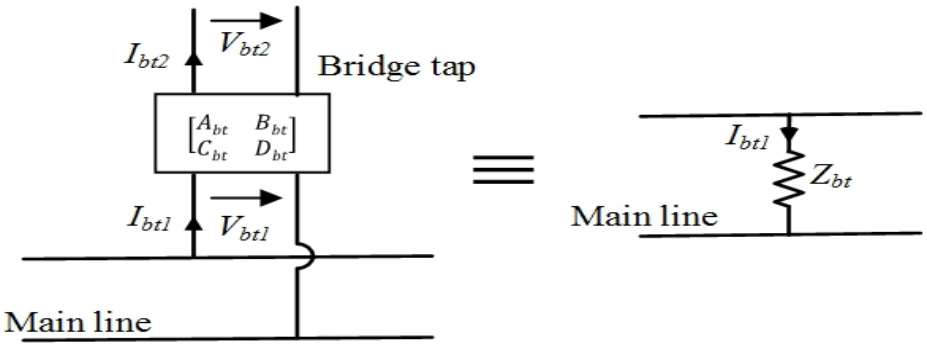

Fig. 5. The equivalent circuit of a bridge tap

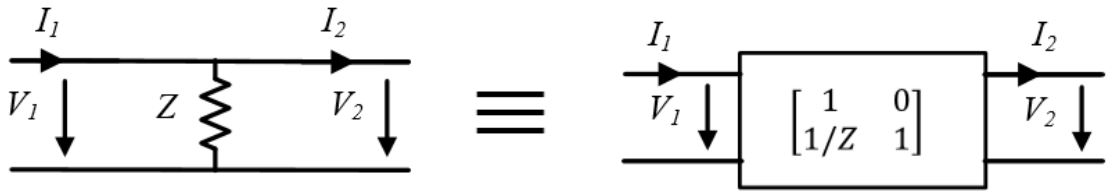

Fig. 6. Transmission matrix of an impedance in parallel

In order to get a transmission matrix of the bridge tap, we need to obtain characteristic impedance of the bridge tap. Because the end of bridge tap is opened, there is no current flow, i.e., $I_{bt2}=0$. Substituting $I_{bt2}=0$ into (14) and (15), the impedance of bridge tap is

$$Z_{bt}=\frac{V_{bt}}{I_{bt}}=Z_{0bt}\coth(\gamma_{bt}l_{bt}) \tag{17}$$

where Z_{0bt} is the characteristic impedance of bridge tap, γ_{bt} is propagation constant and l_{bt} is arbitrary length of bridge tap.

In Fig. 6, the equivalent circuit of the bridge tap can be replaced by a serial two-port network. Using (17), a serial two- port network transmission matrix of the bridge tap is given by

$$T_{bt}=\begin{bmatrix} 1 & 0 \\ \dfrac{1}{Z_{0bt}\coth\left(\gamma_{bt}l_{bt}\right)} & 1 \end{bmatrix}. \tag{18}$$

The cascaded two port network is shown in Fig. 2. The relationship between input voltage and current at port 1 and output voltage and current at port 3 can be expressed as

$$\begin{bmatrix} V_1 \\ I_1 \end{bmatrix}=\begin{bmatrix} A_1 & B_1 \\ C_1 & D_1 \end{bmatrix}\begin{bmatrix} A_2 & B_2 \\ C_2 & D_2 \end{bmatrix}\begin{bmatrix} V_3 \\ I_3 \end{bmatrix} \tag{19}$$

Using this property, the total system transmission parameters can be calculated by

$$T_{total}=T_1T_2T_3T_4\cdots=\prod_{i=1}^{n}T_i \tag{20}$$

Using T_{total}, whole system can be simplified as shown in Fig. 7. Denoting V_S by initial

voltage. The following equation needs to be satisfied [4]

$$V_S = Z_S I_1 + V_1 = A_t V_L + B_t I_L + Z_S \left(C_t V_L + D_t I_L \right) \tag{21}$$

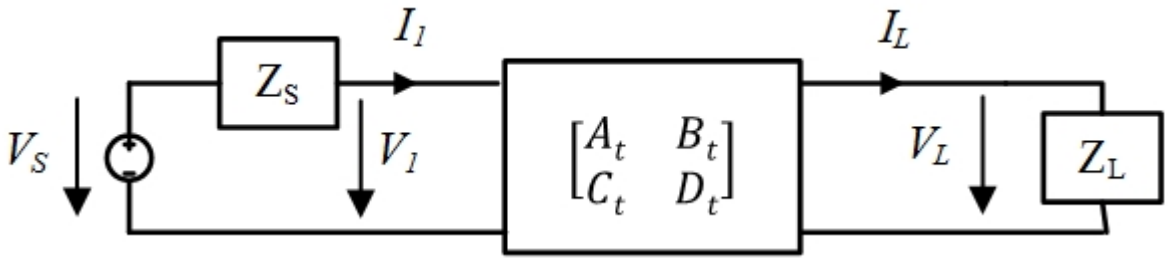

Fig. 7. Total equivalent system schemes with transmission parameters

Using (21), the transfer function of the network is given by

$$H = \frac{V_L}{V_S} = \frac{Z_L}{A_t Z_L + B_t + Z_S \left(C_t Z_L + D_t \right)} \tag{22}$$

4.2. Arbitrary location case

Each ECU can communicate each other because CAN is a multi-master communication system, thus we need to know the channel state between any arbitrary two ECUs. Extending the end-to-end case channel modeling method described in section 4.1, we can figure out the channel response of arbitrary location of the CAN system.

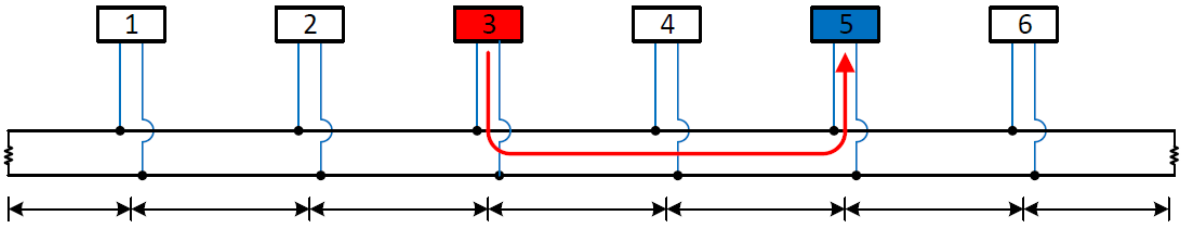

Fig. 8. Configuration of communication between two ECUs

Fig. 8 shows a configuration of communication between two ECUs. In this Figure, ECU 3 transmits CAN signal to ECU 5. The red line shows transmission path of the signal. In order to know channel state between ECU 3 and ECU 5, we need to change the system structure as follows

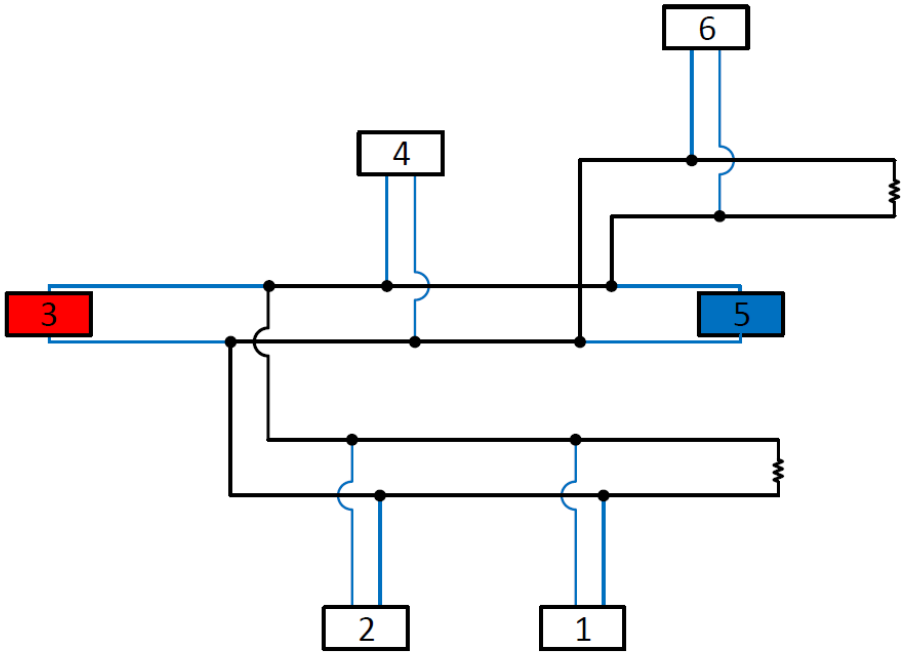

Fig. 9. Changed structure of the Fig. 8

Fig. 9 shows a changed structure of Fig. 8. The left side of bridge tap 4 which includes terminal resistor, bridge tap 1 and bridge tap 2 can be seen as one bridge tap. The right side of bridge tap 4 which includes terminal resistor, bridge tap 6 can be seen as one bridge tap. Thus, we can separate the system into 5 segments as shown in Fig. 10.

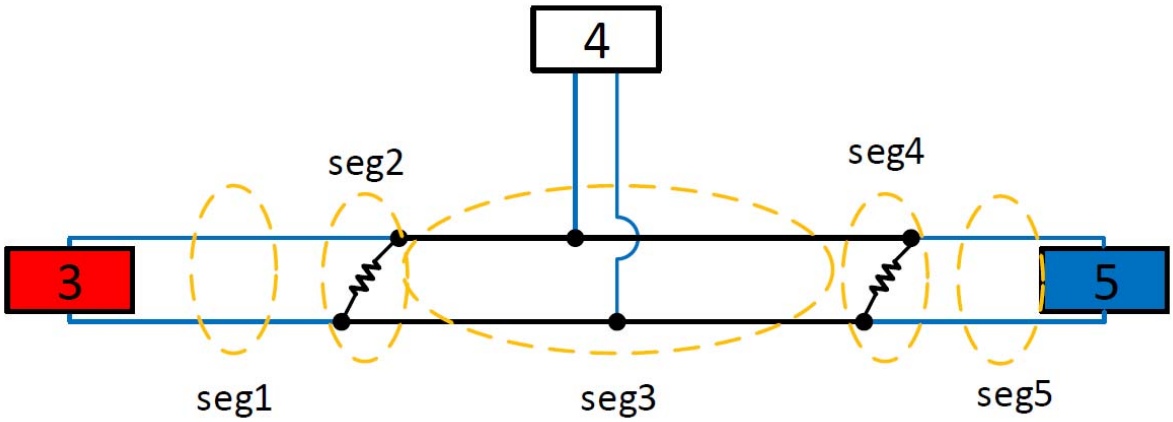

Fig. 10. Equivalent system structure of Fig. 8.

In Fig. 10, the system can be seen as 3 bridge tap CAN system. Then, we can obtain channel modeling result of arbitrary location by using the end-to-end case method which is described

in the previous section.

In 4.1, we obtain a transmission matrix of each line. The main line and the bridge tap can be transformed by a transmission matrix as shown in (16) and (18). In Fig 6, we can get a terminal resistor transmission matrix which is defined as

$$T_{term} = \begin{bmatrix} 1 & 0 \\ \frac{1}{Z} & 1 \end{bmatrix} \tag{23}$$

where Z is terminal resistor of CAN system.

Using (16), (18), (19), (20) and (23) we can get a transmission matrix of each segment. Table 2 shows the procedure of calculation each segment transmission matrix. For the simple calculation of transmission matrix, the main line, *i*-th bridge tap and the terminal resistor transmission matrix are denoted as T_m, T_{bti} and T_{term}, respectively.

Table II. Calculation of T_{segi}

Segment	T matrix	Calculation of T_{Segi}
1	T_{Seg1}	T_m
2	T_{Seg2}	$T_m T_{bt2} T_m T_{bt1} T_{term}$
3	T_{Seg3}	$T_m T_{bt4} T_m$
4	T_{Seg4}	$T_m T_{bt6} T_m T_{term}$
5	T_{Seg5}	T_m

Using Table 2, we can obtain a whole system transmission matrix. In this case, T_{Seg2} and T_{Seg4} can be seen as a bridge tap as shown in Fig. 10. Thus, we have to change the T_{Seg2} and T_{Seg4} into bridge tap transmission matrix form. Denote T_{Seg2} and T_{Seg4} transformed into bridge tap transmission matrix as T_{Seg2bt} and T_{Seg4bt}, respectively.

In Fig 5, V_{bt1} and I_{bt1} given by

$$\begin{bmatrix} V_{bt1} \\ I_{bt1} \end{bmatrix} = \begin{bmatrix} A_{bt} & B_{bt} \\ C_{bt} & D_{bt} \end{bmatrix} \begin{bmatrix} V_{bt2} \\ 0 \end{bmatrix} \tag{24}$$

From (24), it is clear that

$$Z_{bt} = \frac{A_{bt}}{C_{bt}} = Z_{0bt} \coth(\gamma_{bt} l_{bt}) \tag{25}$$

which is same as (17). Using (25), The T_{Seg2} and T_{Seg4} transformed into bridge tap transmission matrix as T_{Seg2bt} and T_{Seg4bt} as

$$T_{Seg\,2bt} = \begin{bmatrix} 1 & 0 \\ \dfrac{C_{Seg\,2}}{A_{Seg\,2}} & 1 \end{bmatrix} \tag{26}$$

$$T_{Seg\,4bt} = \begin{bmatrix} 1 & 0 \\ \dfrac{C_{Seg\,4}}{A_{Seg\,4}} & 1 \end{bmatrix} \tag{27}$$

The whole system transmission matrix can be obtained by

$$T_{system} = T_{seg1} T_{seg\,2bt} T_{seg3} T_{seg\,4bt} T_{seg\,5} \tag{28}$$

Fig. 11 shows transformed structure of Fig. 10. Each segment shown in Fig. 10 transformed into transmission matrix as shown in Fig. 11. Finally, we can obtain a transfer function of the system using (21), (22) and (28)

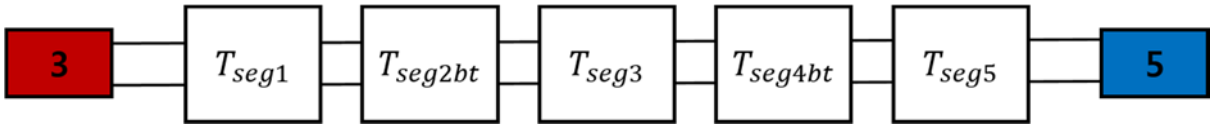

Fig. 11. Transformed structure of Fig. 10.

V. Noise measurement

Not only the transmission characteristic which is affected by the received signal, but also interference or noise characteristics are important factors to calculate channel capacity [8]. To understand the noise characteristics of the CAN system, we need to measure the noise of a real system.

We use the Kia Carens car in order to measure the noise of real CAN system. To measure the noise of real CAN system, we use oscilloscope as the measurement equipment. In Fig. 12, we use connector to extract real CAN signal. The connector from the real CAN system is connected to oscilloscope connector as shown in Fig. 13. Red line is signal line from the real CAN system and black line is ground. Using these connector, we measure the noise of real CAN system with oscilloscope as shown in Fig. 14.

Fig. 12. Connector from the real CAN system

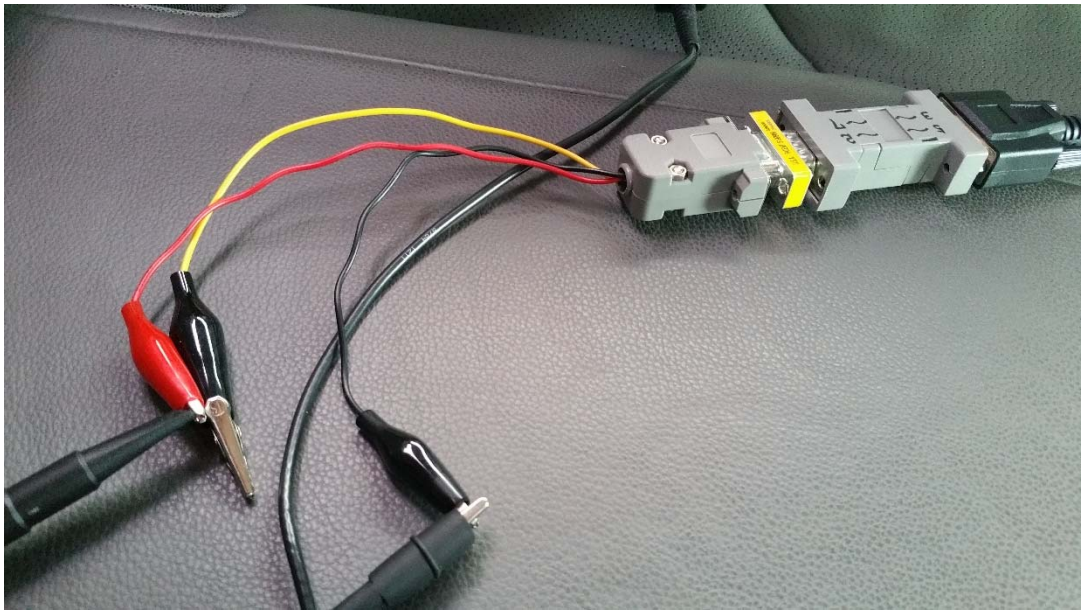

Fig.13. Connector between real CAN system and oscilloscope

Fig. 14. Experiment setup for measuring noise of real CAN system.

Fig. 15 shows generation of the CAN signal. Because traditional CAN system only use baseband for CAN communication, we generated passband CAN signal for analysis of capacity. Using this generated CAN signal, we added Fast fourier transform (FFT) of passband signal to baseband frequency response. The FFT of baseband and passband CAN signal is shown in Fig. 16. In baseband frequency response case, we measure the real CAN signal of the Carens car.

We measure every condition per 100 times. The results are the average value of 100 times measurement.

Using the Fig. 15 and Fig. 16 result, we can get baseband and passband CAN signal in frequency domain. Fig. 17 show the decibel scale of voltage in frequency domain when noise exist.

Finally, using Fig. 16 and Fig. 17, we can get the signal to noise ratio of the real CAN system for capacity calculation as will be shown in section 6.5. Fig. 18 show the SNR of baseband and passband CAN signal.

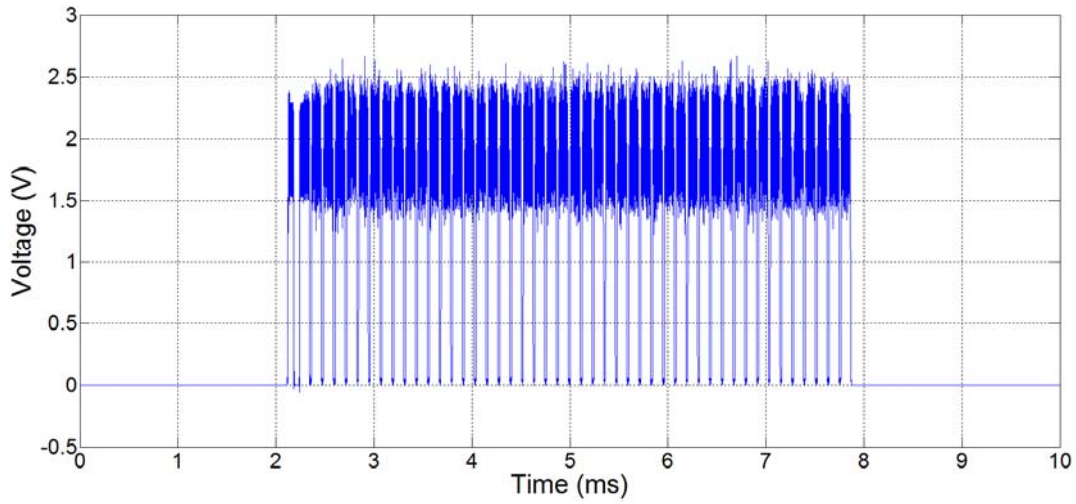

Fig. 15. Generation of passband CAN signal

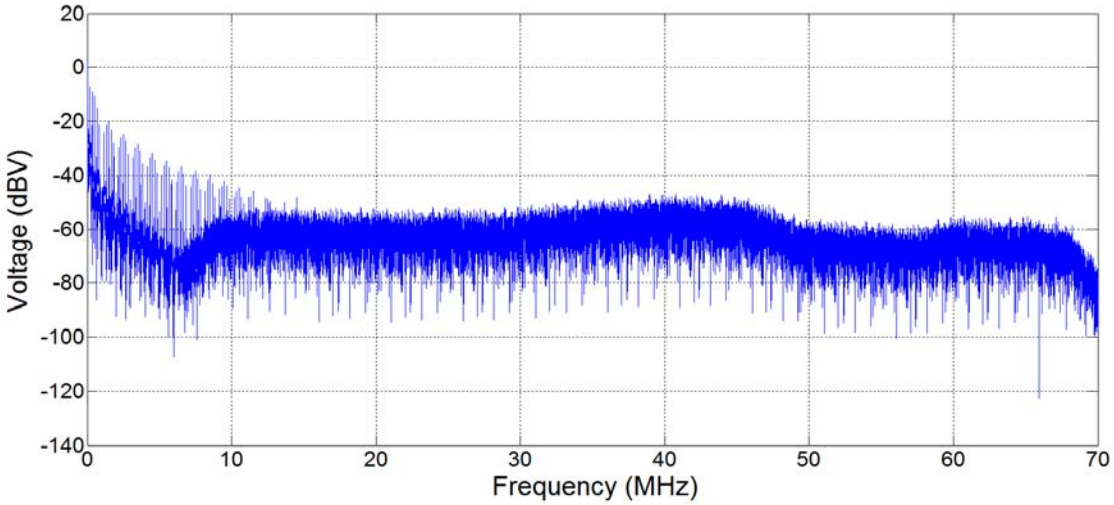

Fig. 16. FFT of baseband and passband CAN signal

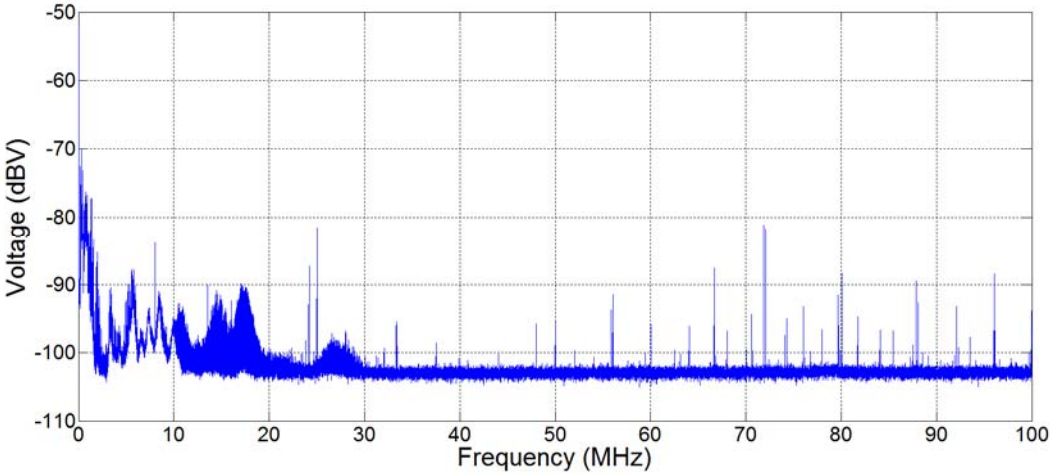

Fig. 17. Decibel scale of voltage in frequency domain when noise exist

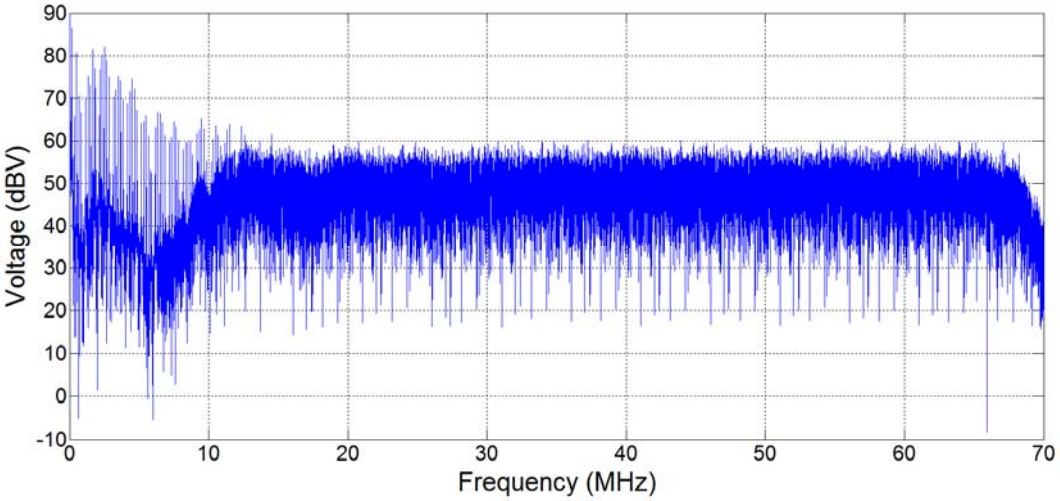

Fig. 18. SNR of baseband and passband CAN signal

VI. Result & Evaluation

6.1. Channel modeling result of end-to-end case

As the number of bridge tap increases, more attenuation and distortion occurs. We consider 1, 4 taps as the best and normal experiment condition and 9 taps as the worst case as shown in Fig. 19. Fig. 19 shows the experiment condition of the CAN system. The bridge tap length varies between 0 cm and 100 cm in 10 cm interval in order to observe the effect of the tap length. The end of bridge tap is open because ECU inside the car has very high impedance. Keysight network analyzer E5061B is used to get a channel response of the CAN system.

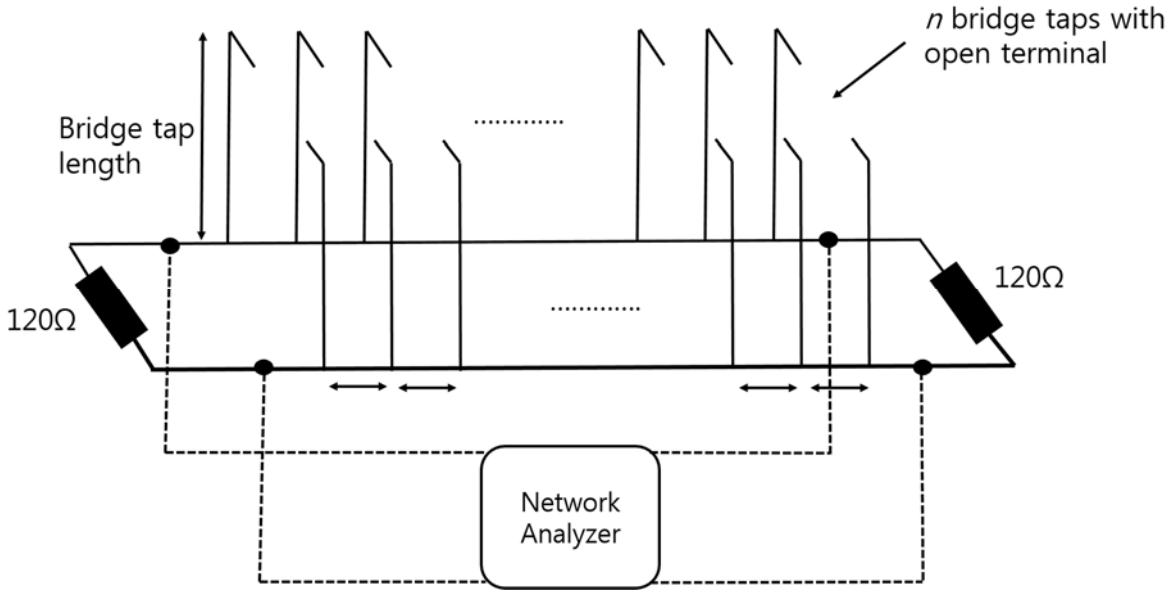

Fig. 19. Experiment condition of CAN system

First, we consider 1 tap as best condition of the CAN system. Fig. 20 ~ Fig. 22 show that path gain with 100 cm, 50 cm and 20 cm in case of 1 tap, respectively. Comparing simulation result with experiment result, although there is slight difference between simulation result and experiment result, we can conclude that the simulation result almost matched with experiment result. Thus, we can approximately know the channel condition by using the simulation.

In case of 100 cm and 50 cm length, main frequency null which experiences high attenuation is generated around 50MHz and 95MHz as shown in Fig. 20 and Fig. 21, respectively. On the other hand, deep frequency null is not observed when the tap length is 20 cm in Fig. 22.

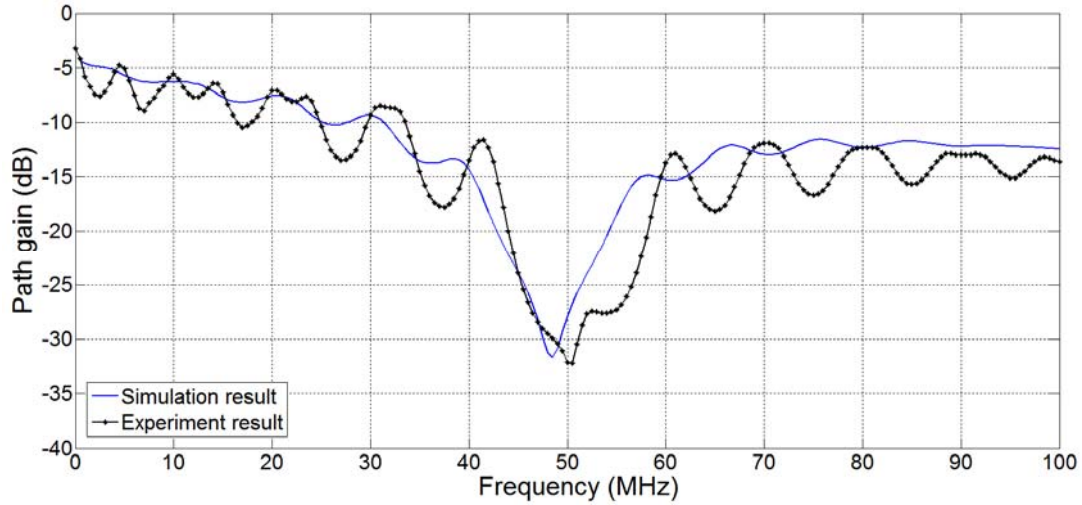

Fig. 20. Path gain with 100 cm bridge tap length (1 tap)

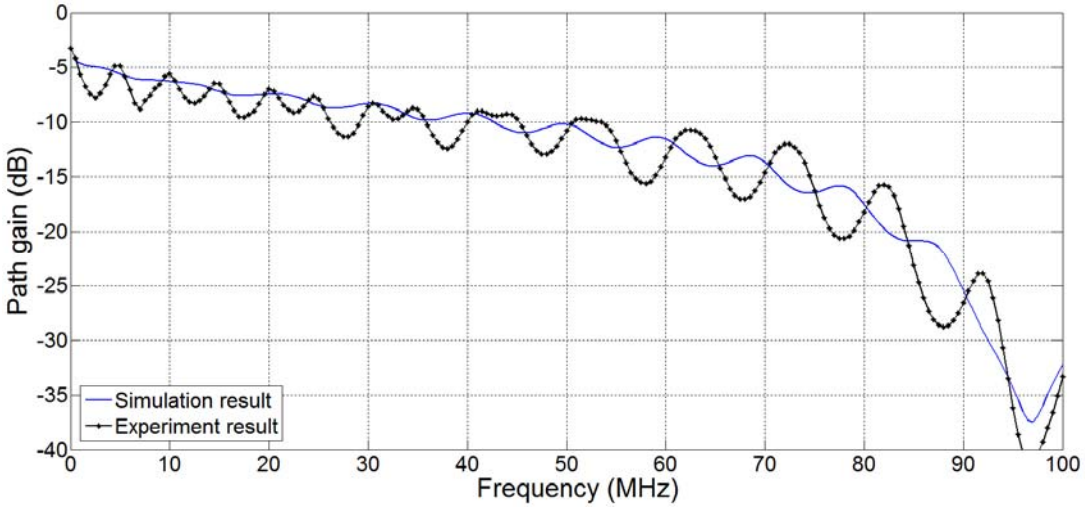

Fig. 21. Path gain with 50 cm bridge tap length (1 tap)

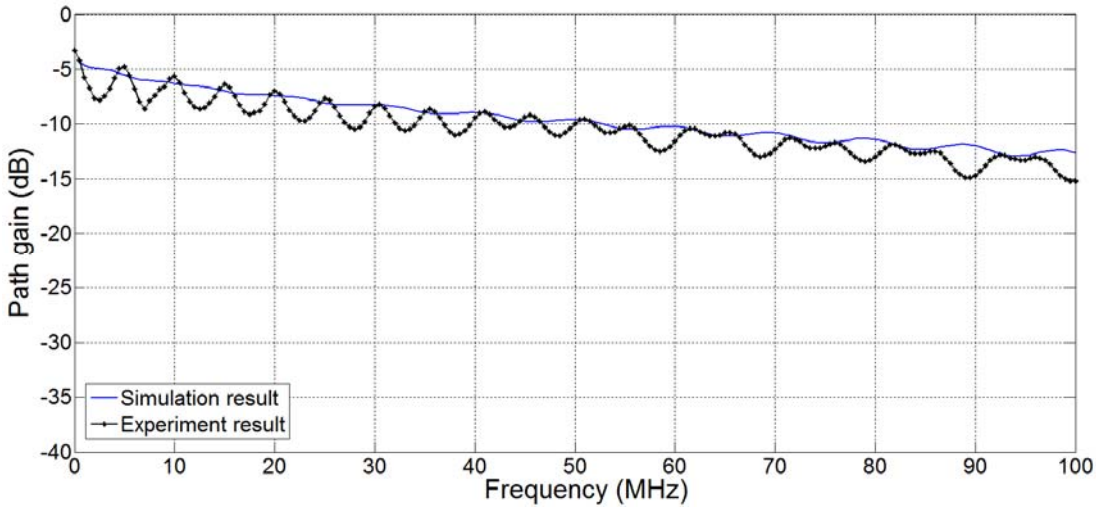

Fig. 22. Path gain with 20 cm bridge tap length (1 tap)

Next, we consider 4 taps as normal condition of the CAN system. Fig. 23 ~ Fig. 25 show that path gain with 100 cm, 50 cm and 20 cm in case of 4 tap, respectively. In case of 100 cm, main frequency null which experiences high attenuation is generated around 50MHz and shallow frequency null is generated around 20MHz and 80MHz. In case of 50cm, shallow and deep nulls are generated around 45MHz, 70MHz and 95MHz. Finally, in case of 20cm, deep frequency null is not observed. Comparing 1 tap case with 4 taps case, the channel condition of 4 taps is worse than 1 tap case. The degree of null generation is deeper and wider than 1 tap case.

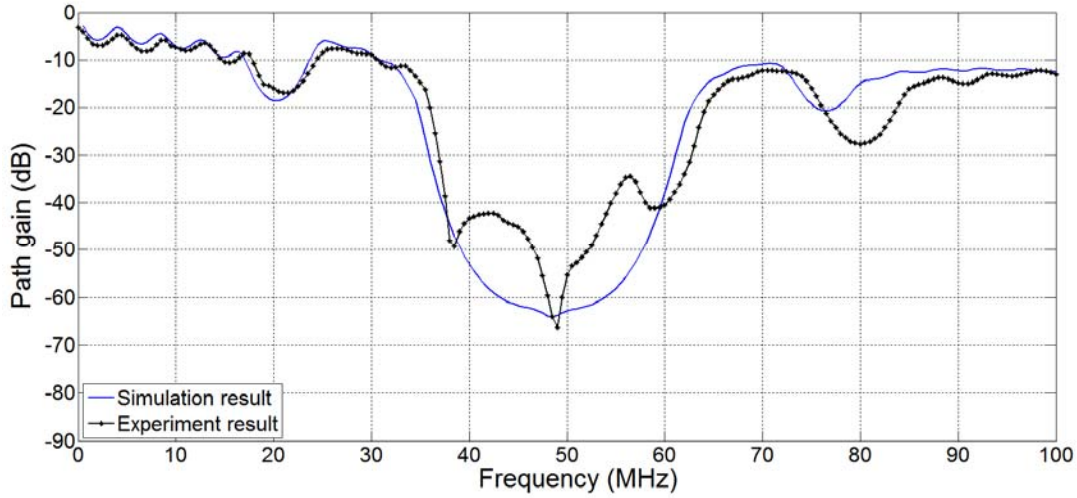

Fig. 23. Path gain with 100 cm bridge tap length (4 taps)

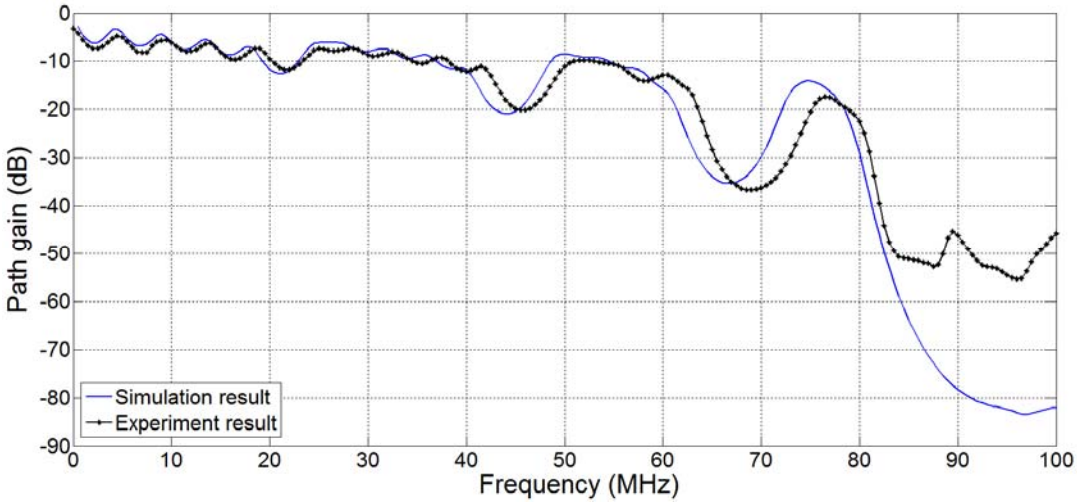

Fig. 24. Path gain with 50 cm bridge tap length (4 taps)

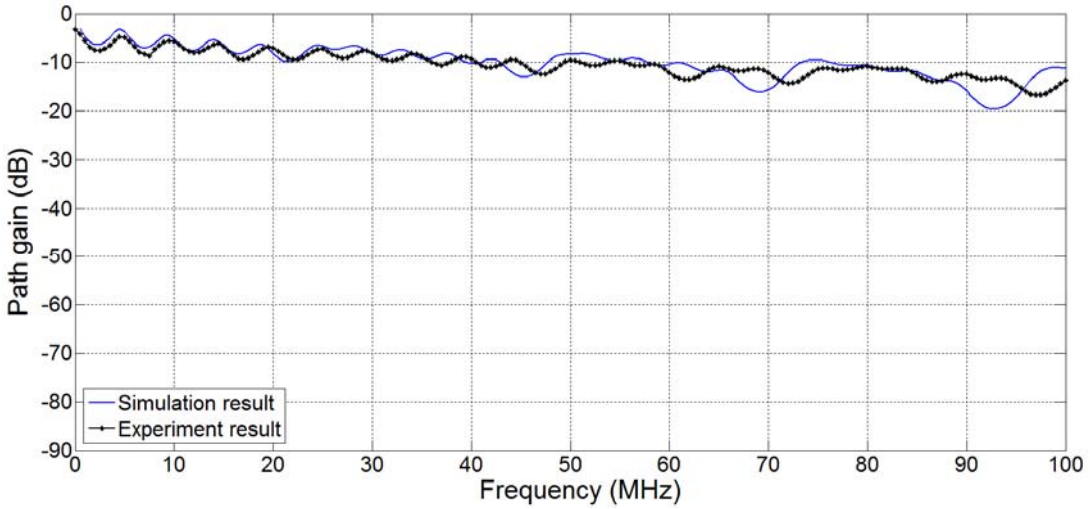

Fig. 25. Path gain with 50 cm bridge tap length (4 taps)

Finally, we consider 9 taps as worst condition of the CAN system. The path gain of the system with 9 taps which have a 100 cm, 50 cm, 20 cm length are shown in Fig. 26, Fig. 27 and Fig. 28, respectively. In case of 100 cm and 50 cm length, main frequency null which experiences high attenuation is generated around 50MHz and 95MHz as shown in Fig. 26 and Fig. 27, respectively. On the other hand, deep frequency null is not observed when the tap length is 20 cm in Fig. 28. Note that significant attenuation lower than -70dB cannot be easily measured in real measurement because wire channel guaranteed good quality of signal transmission, resulting in some difference in null depth in Fig. 26 and Fig. 27. Confirming similar null locations for both the simulation and experimental results through 1 tap, 4 taps and 9 taps case, we can conclude that the proposed channel modeling is quite accurate.

In case of 9 taps attached to the CAN system, the degree of null generation is deeper and wider than 1 tap and 4 taps case. Note that the frequency null moves toward lower frequency band as the length of the bridge tap increases.

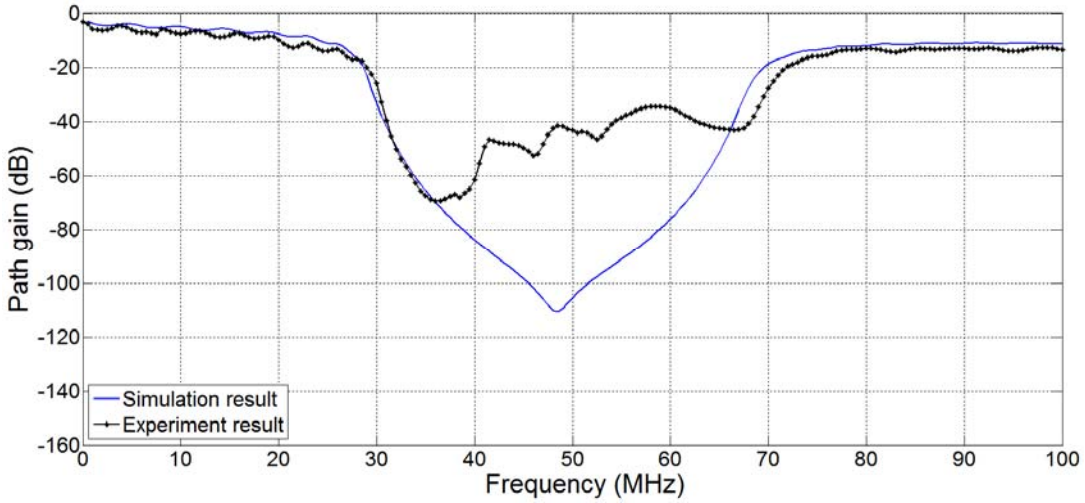

Fig. 26. Path gain with 100 cm bridge tap length (9 taps)

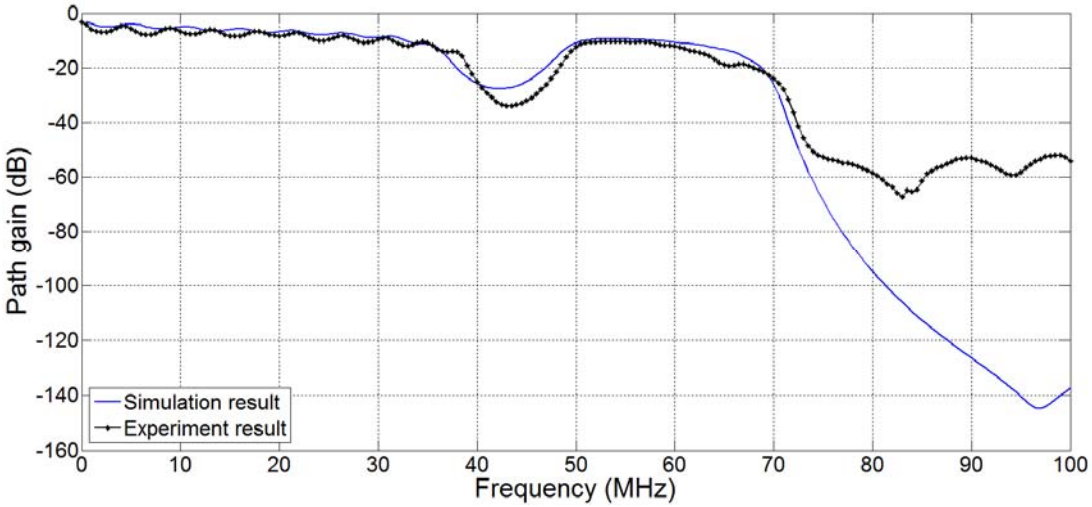

Fig. 27. Path gain with 50 cm bridge tap length (9 taps)

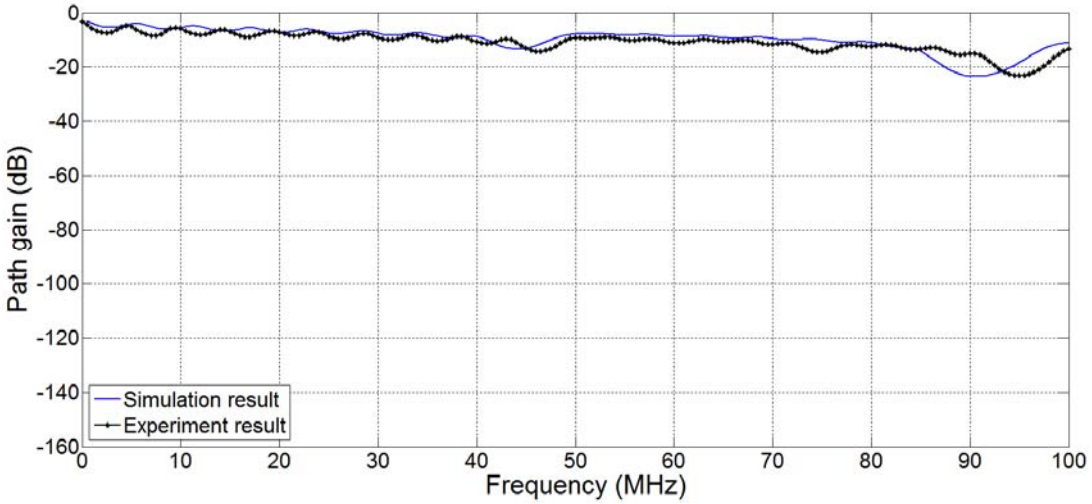

Fig. 28. Path gain with 20 cm bridge tap length (9 taps)

6.2. Channel modeling result of arbitrary Tx-Rx pair

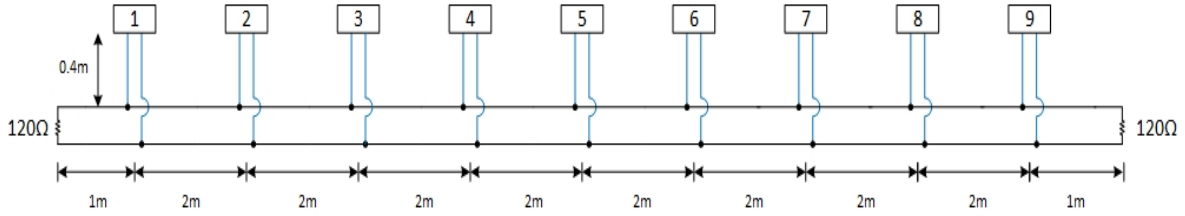

Fig. 29. Configuration of simulation and experiment.

Fig. 29 shows the configuration of simulation and experiment. First of all, we have to check whether simulation result is similar to experiment result. If the channel response of simulation is similar to experiment result when various condition applied, we can know channel response at arbitrary Tx-Rx pair using simulation without experiment result.

We compared simulation result with experiment result in various condition as shown in Fig. 30 ~ Fig. 35. Each bridge tap is separated by 2 m interval and each bridge tap length is 0.4 m. Fig. 30 shows path gain between bridge tap 3 and bridge tap 4 which is the closest distance between transmitter and receiver. Confirming similar null locations for both simulation and experimental results through Fig. 30 ~ Fig. 35, we can conclude that the proposed channel modeling is quite accurate in case of arbitrary Tx-Rx pair.

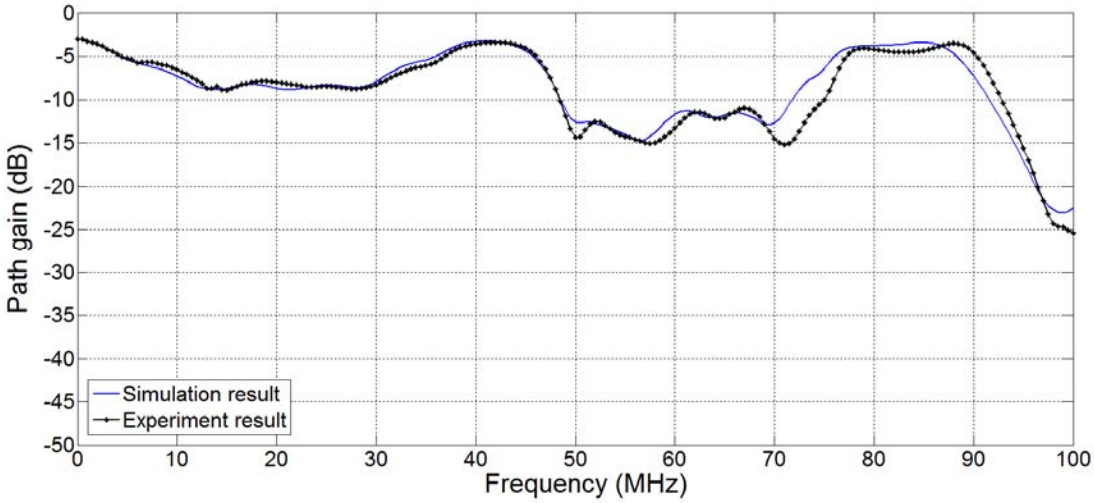

Fig. 30. Path gain between bridge tap 3 and bridge tap 4

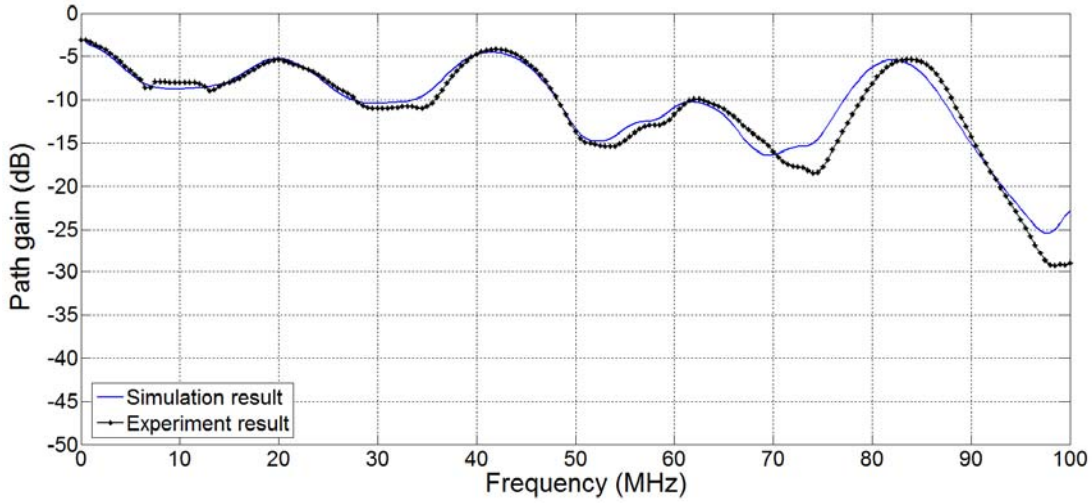

Fig. 31. Path gain between bridge tap 3 and bridge tap 5

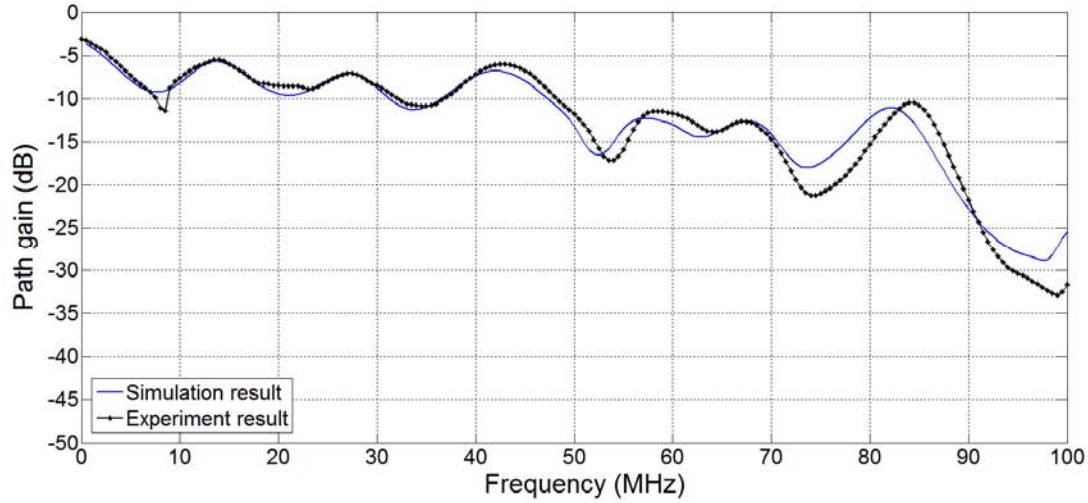

Fig. 32. Path gain between bridge tap 3 and bridge tap 6

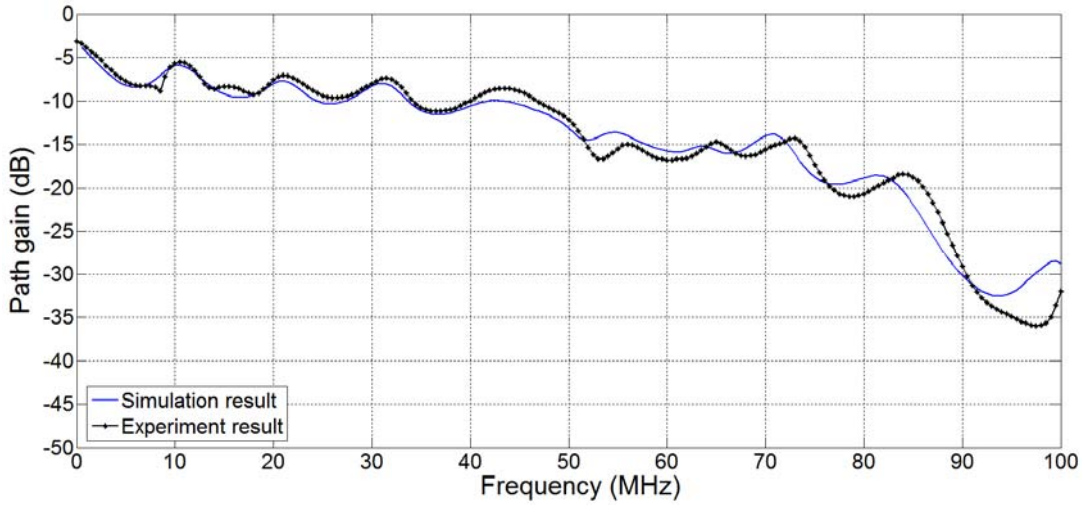

Fig. 33. Path gain between bridge tap 2 and bridge tap 6

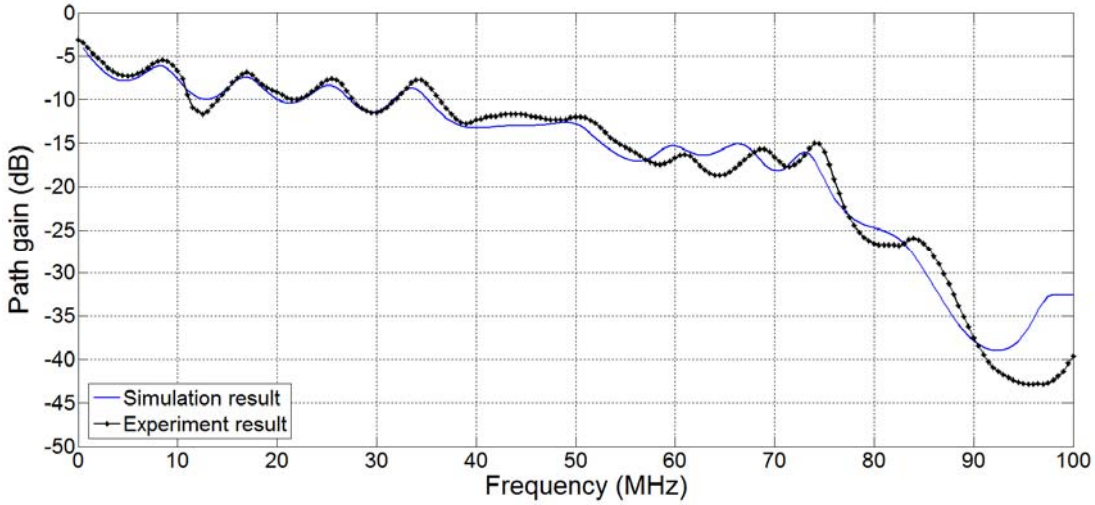

Fig. 34. Path gain between bridge tap 2 and bridge tap 7

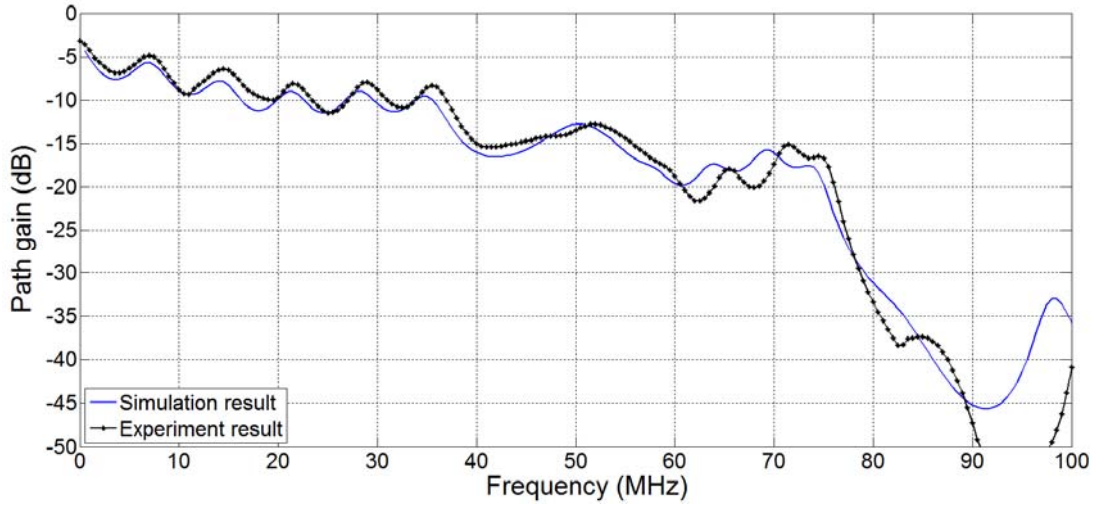

Fig. 35. Path gain between bridge tap 2 and bridge tap 8

We use the simulation result in order to check channel response of CAN system without experiment as shown in previous part because we already had checked the similarity between simulation result and experiment result. Fig. 36 ~ Fig. 38 are path gain result using simulation in case of Tx = 1.

Fig. 36, Fig. 37 and Fig 38 show the path gain in case of Tx = 1 when bridge tap length is 100 cm, 50 cm and 20 cm, respectively. In Fig. 36 which have longest bridge tap length among the Fig 36 to Fig 38, the main deep frequency null is generated around 50MHz. As the distance between Tx and Rx increased, the generated null is deeper and wider. Path gain in case of Tx=1 with 50 cm bridge tap length is shown in Fig. 37. Same as end-to-end case, the frequency null moves toward lower frequency band as the length of the bridge tap increases. We can also

check that the distance between Tx and Rx increased, the generated null is deeper and wider in Fig. 37. The channel response in case of Tx=1 with 20 cm bridge tap length is shown in Fig. 38. Among the 100cm, 50cm and 20cm, the 20cm case is best condition of channel. The channel condition is relatively flat than other bridge tap length.

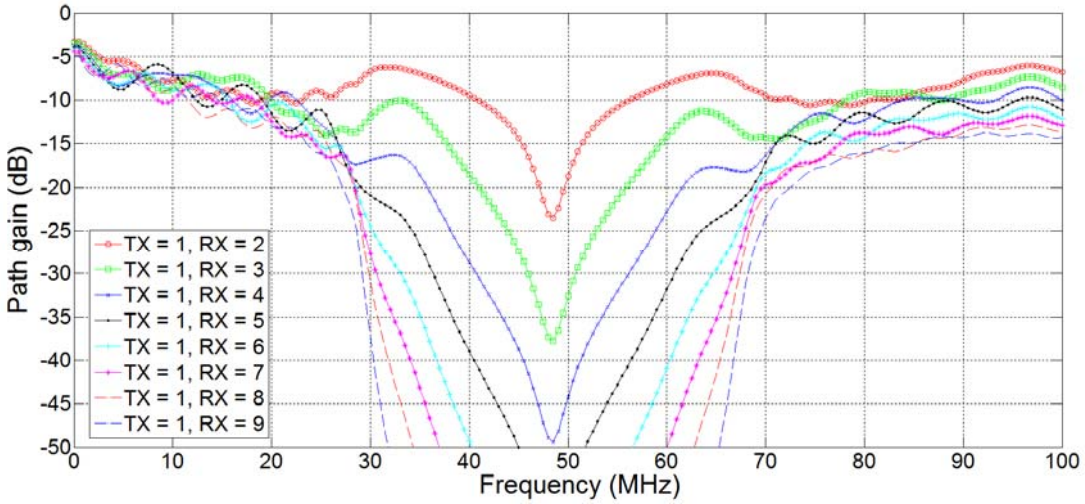

Fig. 36. Path gain in case of Tx = 1 (bridge tap length = 100cm)

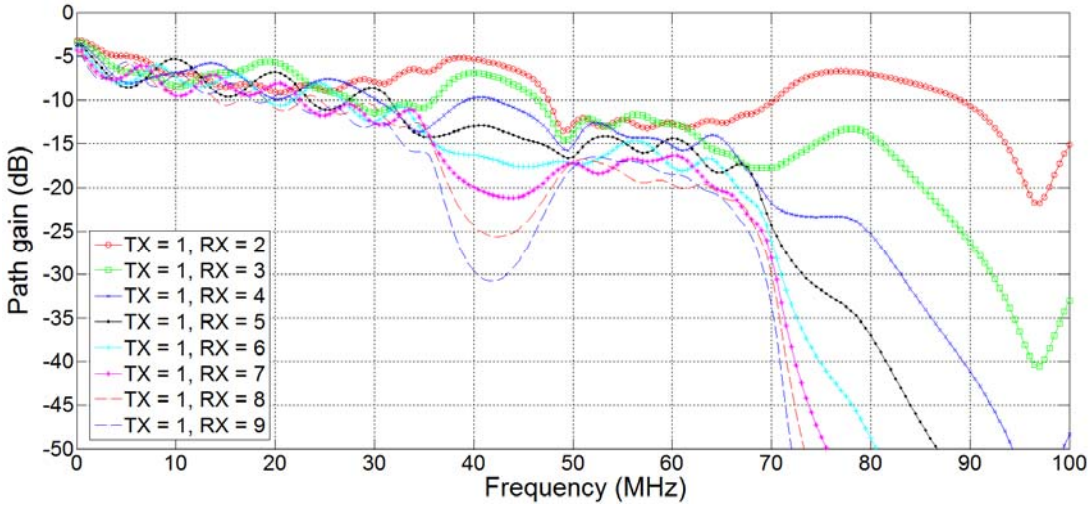

Fig. 37. Path gain in case of Tx = 1 (bridge tap length = 50cm)

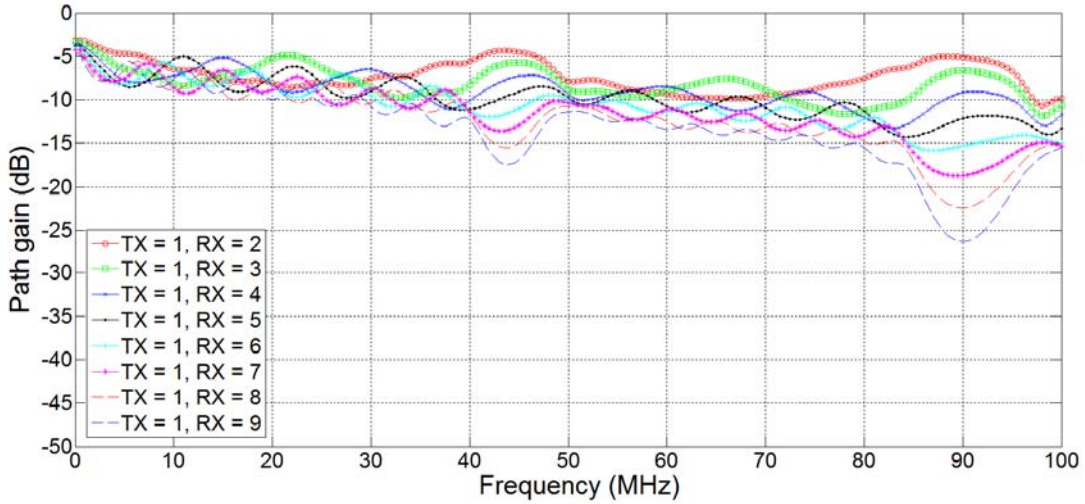

Fig. 38. Path gain in case of Tx = 1 (bridge tap length = 20cm)

Fig. 39, Fig. 40 and Fig 41 show the path gain in case of Tx = 2 when bridge tap length is 100 cm, 50 cm and 20 cm, respectively. Comparing Tx=1 with 100 cm bridge tap length, the generated frequency null is deeper than Tx=1 case. We can also check the tendency of null generation in case of Tx=2 is similar to Tx=1 case. Besides, we can check if the number of bridge tap between Tx and Rx same, the shape and the magnitude of channel response similar regardless of Tx and Rx position.

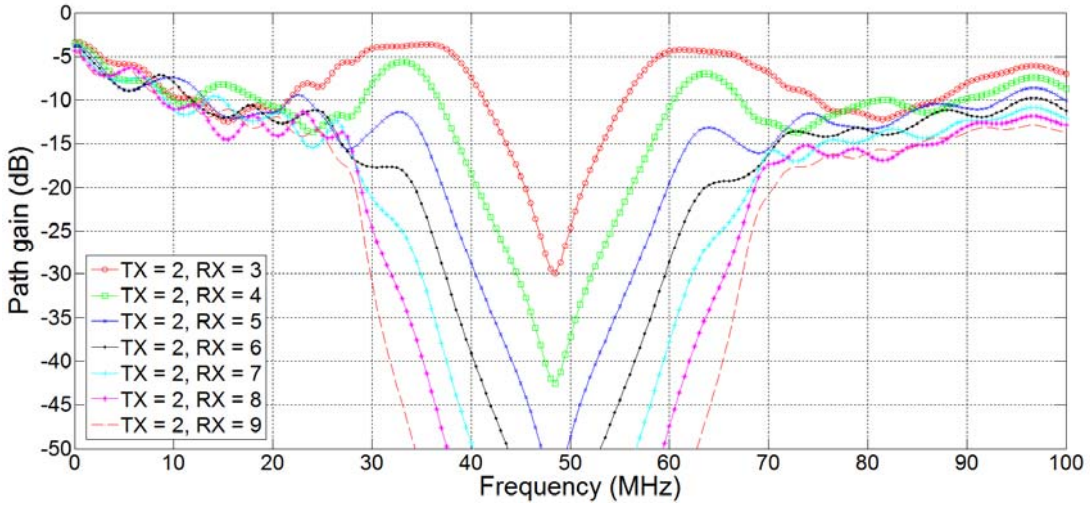

Fig. 39. Path gain in case of Tx = 2 (bridge tap length = 100cm)

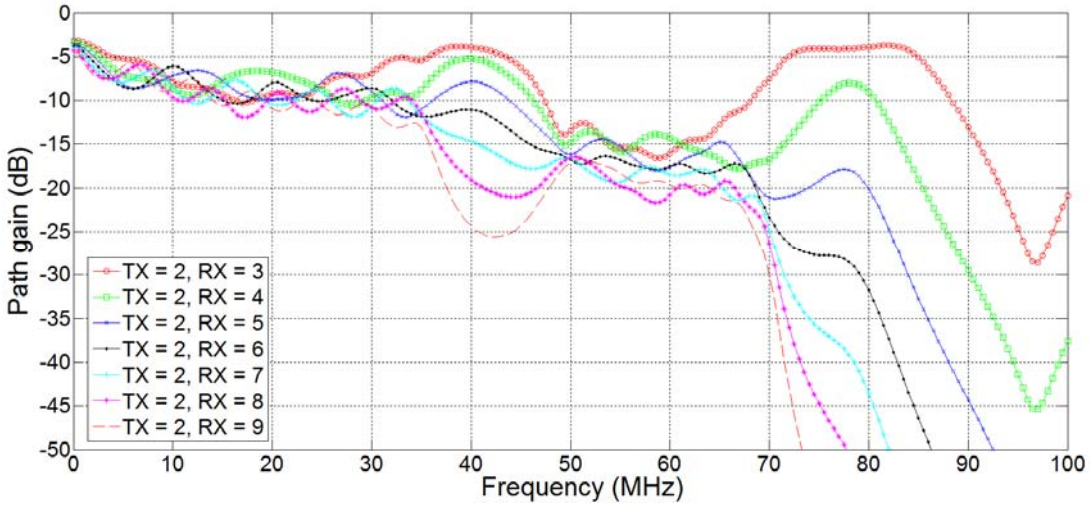

Fig. 40. Path gain in case of Tx = 2 (bridge tap length = 50cm)

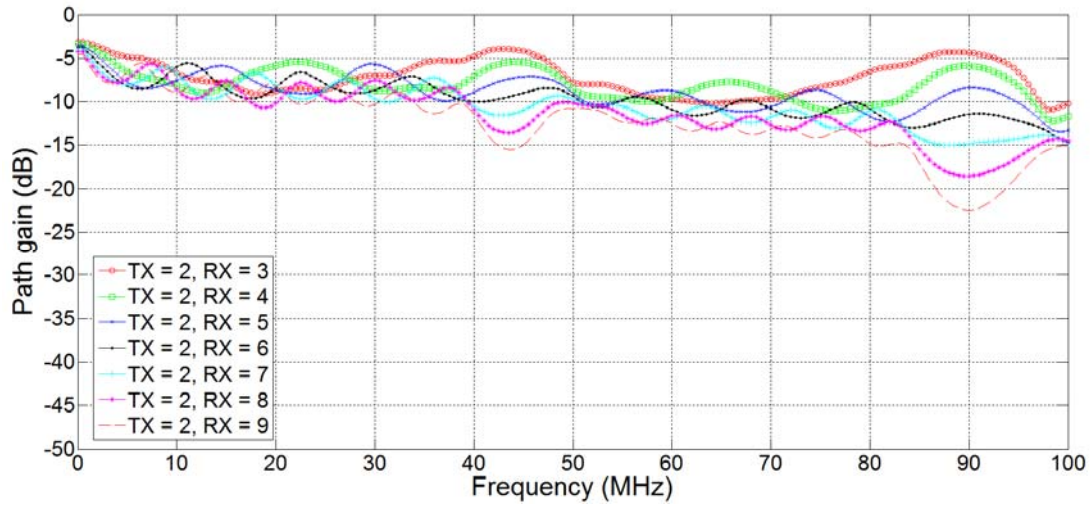

Fig. 41. Path gain in case of Tx = 2 (bridge tap length = 20cm)

Fig. 42, Fig. 43 and Fig 44 show the path gain in case of Tx = 3 when bridge tap length is 100 cm, 50 cm and 20 cm, respectively. In case of Tx=3, the tendency and the magnitude of null generation is similar to Tx=2 case. Thus, we check again the distance between Tx and Rx increased, the generated null is deeper and wider and the number of bridge tap between Tx and Rx same, the shape and the magnitude of channel response are similar regardless of Tx and Rx position.

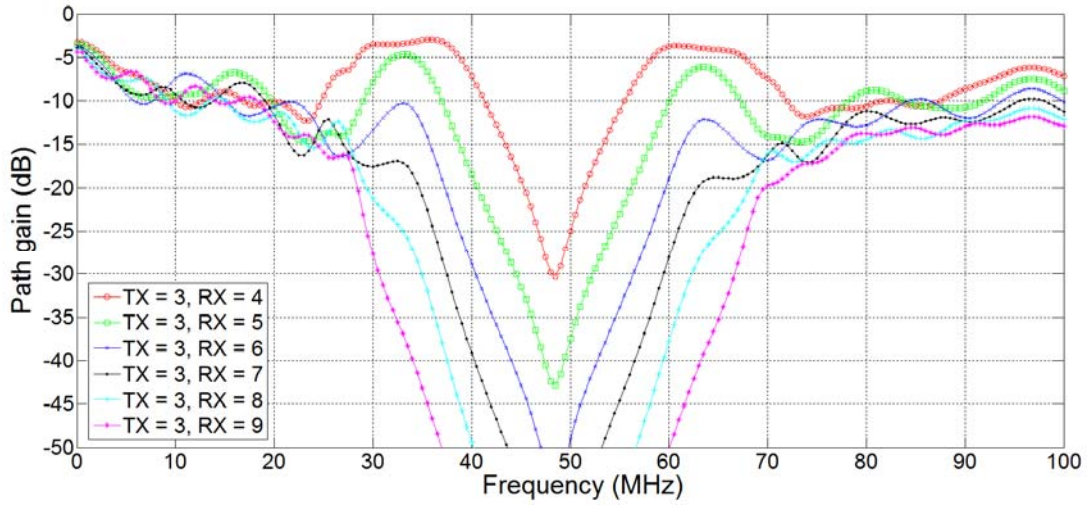

Fig. 42. Path gain in case of Tx = 3 (bridge tap length = 100cm)

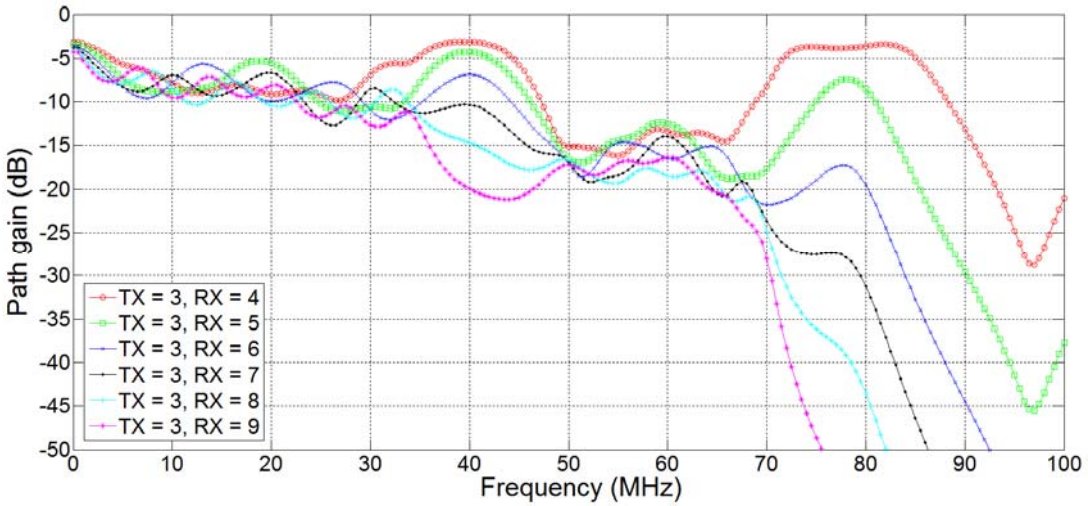

Fig. 43. Path gain in case of Tx = 3 (bridge tap length = 50cm)

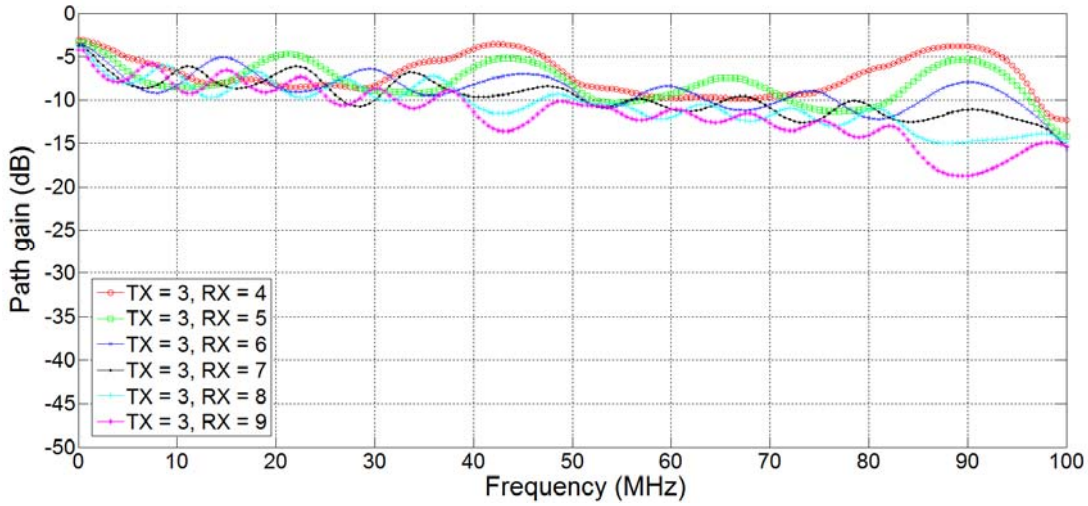

Fig. 44. Path gain in case of Tx = 3 (bridge tap length = 20cm)

Finally, Fig. 45, Fig. 46 and Fig 47 show the path gain in case of Tx = 4 when bridge tap length is 100 cm, 50 cm and 20 cm, respectively. As we expected, the tendency and the magnitude of null generation is similar to Tx=2 and Tx=3 cases.

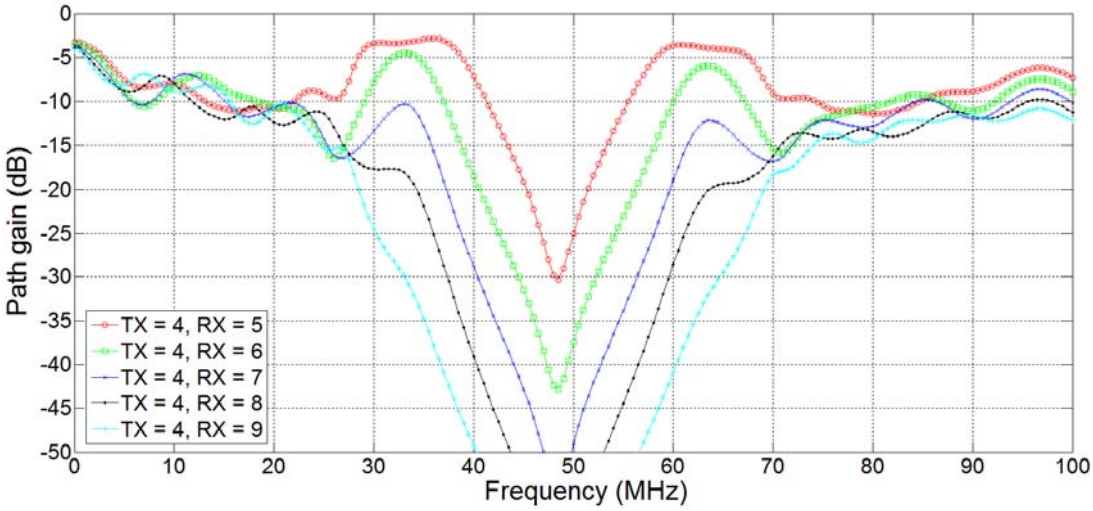

Fig. 45. Path gain in case of Tx = 4 (bridge tap length = 100cm)

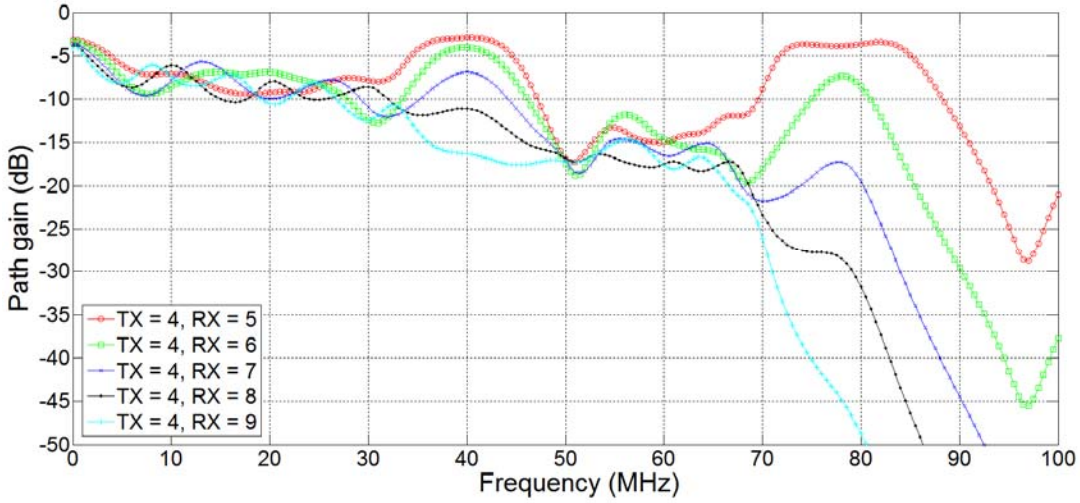

Fig. 46. Path gain in case of Tx = 4 (bridge tap length = 50cm)

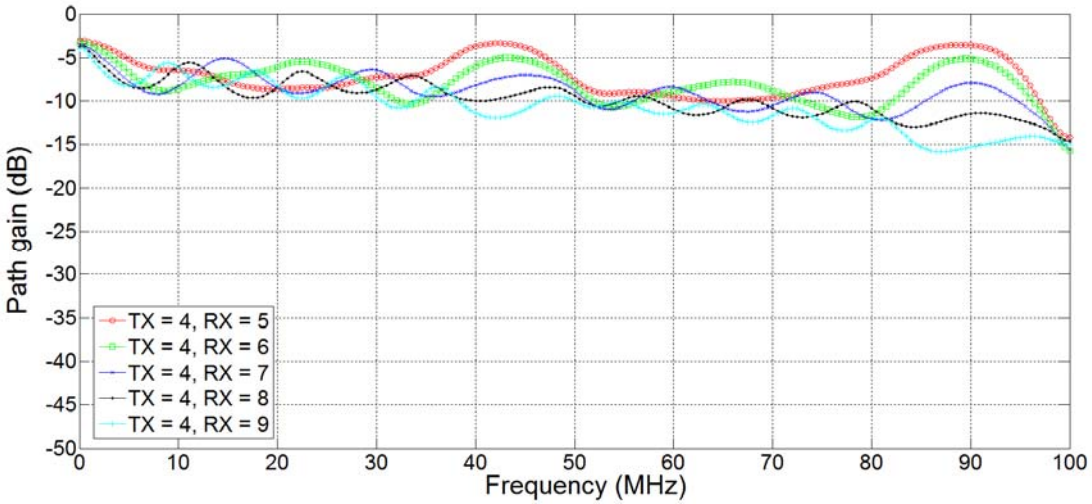

Fig. 47. Path gain in case of Tx = 4 (bridge tap length = 20cm)

6.3. Evaluation of channel modeling result

In end-to-end case, from the previous section, we checked the degree of null generation is deeper and wider as the number of tap increased. Note that the frequency null moves toward lower frequency band as the length of the bridge tap increases. From this result, we suggest frequency band between 20MHz and 70MHz and a tap length less than 50 cm allowing up to 50dB loss for designing CAN communication systems in case of end-to-end. The available bandwidth for passband communication already described in Section III.

Channel attenuation is affected by bridge tap length not only end-to-end case, but also the arbitrary Tx-Rx pair case. But, different from end-to-end case, we can check the relationship between channel response and Tx-Rx pair location. From Fig. 36 ~ Fig 47, it is clear that the distance between Tx and Rx increased, the generated null is deeper and wider. Besides, if the number of bridge tap between Tx and Rx same, the shape and the magnitude of channel response are similar regardless of Tx and Rx position. Same as end-to-end case, we suggest frequency band between 20MHz and 70MHz and a tap length less than 50 cm allowing up to 50dB loss for designing CAN communication systems in case of arbitrary Tx-Rx pair.

Using these properties, when designing CAN system considering with priority of ECUs signal transmission, we can design CAN system structure by changing bridge tap length and location of Tx and Rx. If one of the ECU have a highest priority in the CAN system, we have to use shortest bridge tap and location of transmitter must be placed in closest distance to receiver when we design the CAN system.

6.4. Impulse response of arbitrary Tx-Rx pair

In order to know which signal transmission path is dominant, we need to analyze time-domain impulse response of arbitrary Tx-Rx pair. Because we see experiment result almost matched with simulation result as shown in 6.2, we use the simulation result to analyze impulse response of arbitrary location.

In time domain, when the transmitted signal passed through channel, received signal is defined as [9]

$$y(t) = h(t) * x(t) + n(t) \tag{29}$$

where *h(t)* is channel impulse response in time domain, *x(t)* is transmitted signal and *n(t)* is noise.

In order to obtain channel impulse response in time domain, we use channel response in frequency domain which is described in previous section. Using this channel response, we can obtain time-domain impulse response by using inverse fast fourier transform (IFFT) method. The IFFT is the tool which convert channel response in frequency domain into channel impulse response in time domain [9]. We use Fig. 48 (Tx=3) to analyze impulse response.

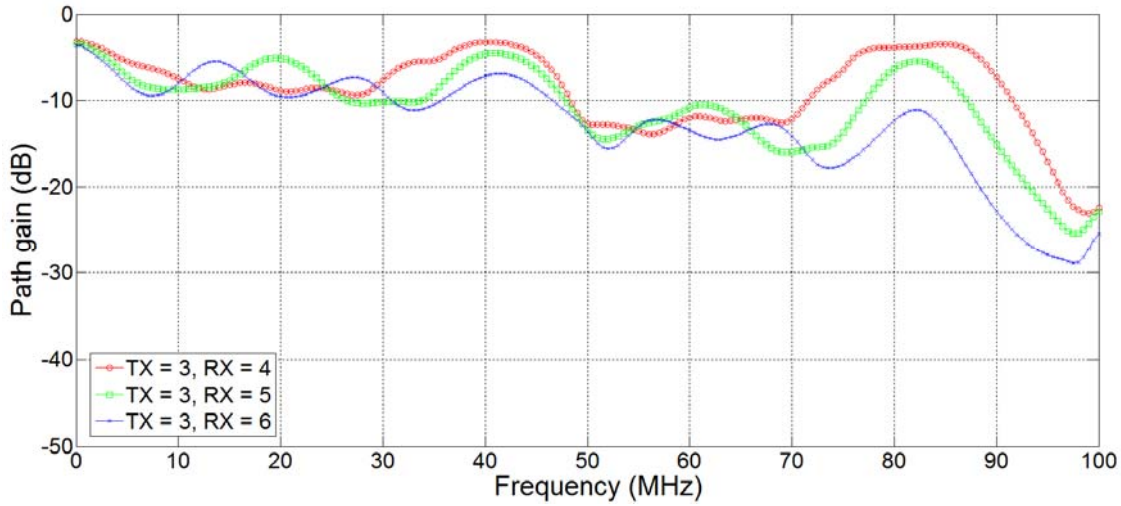

Fig. 48. Path gain in case of Tx = 3 (bridge tap length = 40cm)

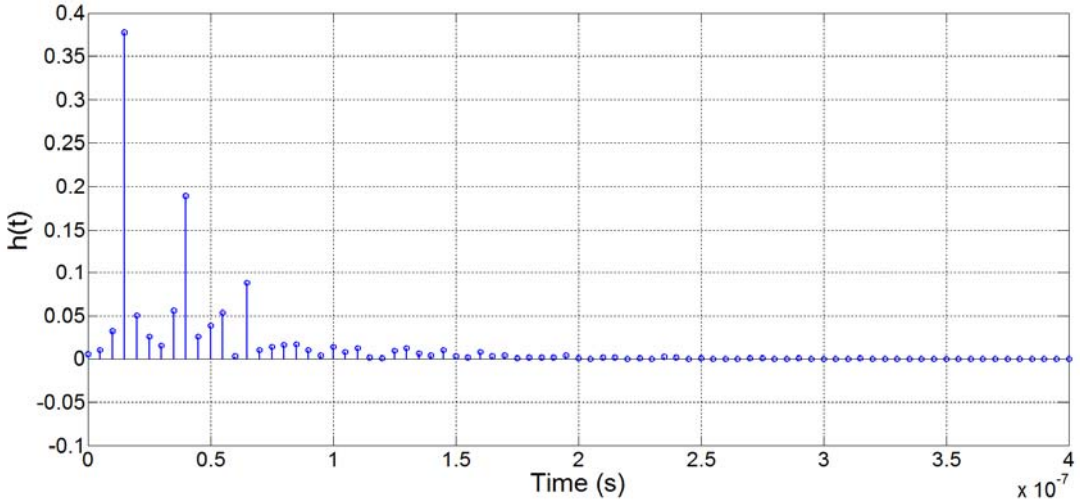

Fig. 49. Impulse response of Tx=3, Rx=4

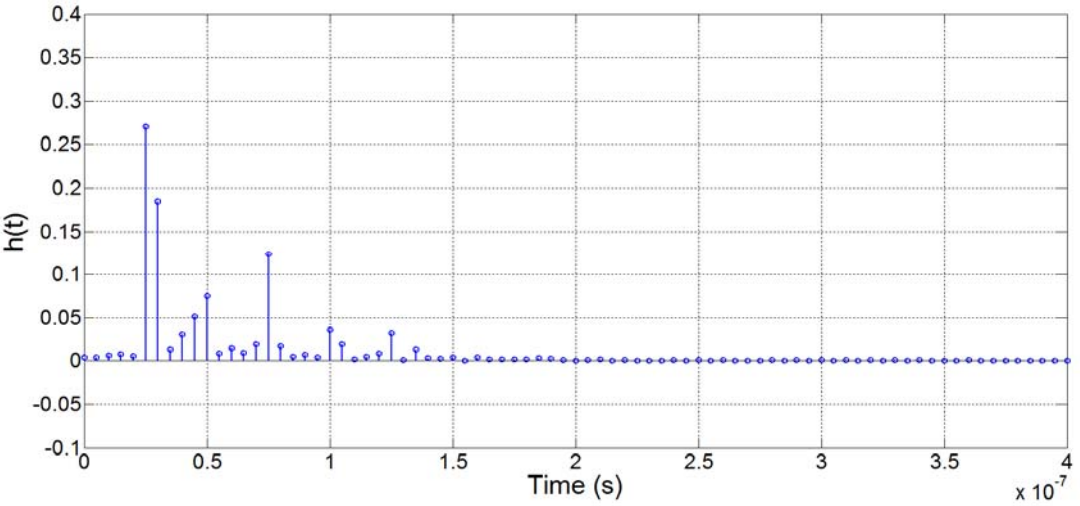

Fig. 50. Impulse response of Tx=3, Rx=5

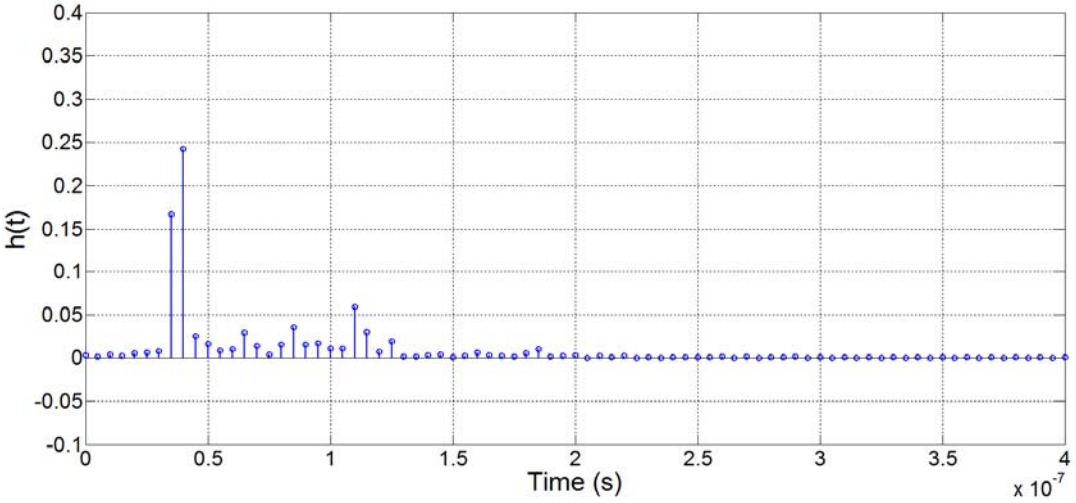

Fig. 51. Impulse response of Tx=3, Rx=6

Table III. Delay and *h(t)* of impulse response in time domain

Number of Figure	First path		Second path		Third path	
	h(t)	delay	*h(t)*	delay	*h(t)*	delay
Fig. 32	0.377	15ns	0.189	40ns	0.087	65ns
Fig. 33	0.270	25ns	0.184	30ns		
Fig. 34	0.167	35ns	0.242	40ns		

Fig. 48 ~ Fig. 51 plots impulse response in time domain using simulation result. Table 3 shows the *h(t)* and delay of first, second and third dominant signal transmission path of the CAN system. To know which path is dominant, we compared to calculated result. The speed of light in copper is about 66% ± 2% of the light speed in free space [10][11]. We use 64% of light speed in free space, i.e., $v_{copper} = 1.92 \times 10^8$ m/s. In Fig. 32, the distance of first path, second path and third path are $1.92 \times 10^8 (m/s) \times 1.5 \times 10^{-8} (s)$ = 2.88 m, 7.68 m and 11.52 m, respectively. In Fig. 29, we can calculate each path distance. The calculated first path distance is 2.8m which is direct direction from Tx 3 to Rx 4. Table 4 shows calculated each path distance, direction and simulation distance. Comparing simulation distance with calculated distance, we can conclude that the simulation results are quite accurate. From this result, we conclude that the first dominant path is affected by direct path of signal transmission and the second dominant path is affected by closest bridge tap to transmitter.

Table IV.

The result of comparing the simulation distance with the calculated distance

Num. Fig	Path	Simulation distance	Direction (distance)
Fig. 49	First	2.88m	3→4 (2.8m)
	Second	7.68m	(3→2→4) + (3→5→4) (7.6m)
	Third	11.52m	(3→1→4) + (3→6→4) (11.6m)
Fig. 50	First	4.8m	3→5 (4.8m)
	Second	5.76m	3→4→5 (5.6m)
Fig. 51	First	6.72m	3→6 (6.8m)
	Second	7.68m	(3→4→6) + (3→5→6) (7.6m)

6.4. Capacity analysis

In order to know maximum data rate of the CAN system, we have to analyze capacity. The channels are separated into k narrow flat band flat fading subchannels of span Δf . The capacity of *i* th subchannel is defined as [12]

$$C_i = \frac{1}{2}\log_2(1+\frac{P_i|H(f)|^2}{\sigma_i^2}) \tag{30}$$

where H(*f*) is frequency response of the channel, P_i is the transmitted signal power and σ_i^2 is the noise power . Note that we already know the signal to noise ratio (SNR) as seen in Section V. The total channel capacity is defined as

$$C = 2\Delta f \sum_{i=0}^{k-1} C_i. \tag{31}$$

If k goes to infinite, the total channel capacity is defined as [13]

$$C = \int_0^{BW} \log_2(1+\frac{P(f)|H(f)|^2}{N_0})df \tag{32}$$

where BW is the frequency bandwidth and N_0 is noise power.

Using (30), (31) and (32), we can calculate capacity of the CAN system. Using Fig. 43 channel response and noise measurement result as shown in section 5, we can obtain a capacity. Table 5 shows capacity of each Tx-Rx pair with considering channel condition in Fig. 43.

Table V. Capacity of each Tx-Rx pair

Num. Fig	Bandwidth	Tx	Rx	Capacity (Gbps)
Fig. 43 (Tx=3 with 50 cm bridge tap)	20-70 MHz	3	4	1.331
			5	1.215
			6	1.174
			7	1.197
			8	1.205
			9	1.191

From this table, we can know the capacity of each Tx-Rx pair condition with considering the channel condition. In case of considering 20-70 MHz bandwidth, we can use over around 1G bps for data transmission of CAN system. Although considering the payload, it is clear that the achievable data rate of CAN system is over than 100Mbps.

VII. Conclusion

In this paper, we described the channel modeling of CAN communication using a transmission matrix and verified it through experiments. By multiplication of each transmission matrix, we obtained the total transmission matrix and the transfer function of the system. Based on the proposed method, we can obtain the channel frequency response which can be used for decision of suggested tap length and bandwidth without real measurements. Using this channel modeling result, we get an impulse response and capacity of the system. By using this result, we can know which signal transmission path is dominant and maximum data rate of the system.

In future work, we will consider analyzing the performance and designing of CAN communication systems. Using the channel response and capacity analysis result, we can determine appropriate modulation scheme, and design equalizers.

Reference

[1] M. Farsi, K. Ratcliff, and M. Barbosa, “An overview of controller area network,” *Comput. Control Eng. J.*, vol. 10, no. 3, pp. 113–120, Aug. 1999.

[2] F. Hartwich, “CAN with Flexible Data-Rate,” In *13th International CAN Conf*., Hambach., Germany, 2012.

[3] S. Nitta, D. Umehara, K. Wakasugi, S. Ishiko, and T. Tsubouchi, “High rate and high multiplexing CAN by short pulse line codes,” In *Proc. IEEE VTC Spring*, 2013.

[4] National Instruments (2009). *Flexray Automotive Communication Bus Overview*. Available : http://www.ni.com/white-paper/3352/en/

[5] D. Paret and R. Riesco, *Multiplexed Networks for Embedded Systems: CAN, LIN, Flexray, Safe-by-Wire*, SAE Int’l., 2007

[6] P. Golden, H. Dedieus and K. Jacobsen, *Fundamentals of DSL technology*, New York: Auerbach, pp. 41-78, 2006.

[7] R. F. M. van de Brink, “Cable reference models for simulating metallic access networks,” ETSI, TM6 Permanent Document TM6(97)02, June. 1998.

[8] M. Gotz, M. Rapp, and K. Dostert, “Power line channel characteristics and their effect on communication system design,” *IEEE Commun. Mag*., vol. 42, no. 4, pp. 78–86, Apr. 2004.

[9] A. V. Oppenheim and A. S. Willsky, *Signals and Systems*. 2nd ed. Englewood Cliffs, NJ: Prentice-Hall, 1997.

[10] K. L. Kaiser, “Transmission Lines, Matching, and Crosstalk,” CRC Press, Sep. 2005.

[11] K. Hirabayashi. (2001). *Phase velocity of electromagnetic waves and medium constants*. Available : http://www.mogami-wire.co.jp/e/puzzle/pzl-18.html.

[12] P. Langfeld, “The capacity of typical power line channels and strategies for system design,” *Proc. 5th Int’l. Symp. Power-Line Commun*., Malmö, Sweden, pp. 271-78, 2001.

[13] D. Tse and P. Viswanath, *Fundamentals of Wireless Communications*. Cambridge, U.K.: Cambridge Univ. Press, 2005.

요 약 문

Controller Area Network (CAN) 통신 채널 모델링 및 커패시티 분석

Controller area network (CAN) 는 신호의 제어가 쉽고 오류에 강인한 특성 때문에 자동차 내부 통신 프로토콜로 많이 사용되며, 최대 1Mbps 의 데이터 전송률을 제공한다. 하지만, 자동차 내부의 전자장치들이 증가함에 따라 높은 데이터 전송률이 필요하게 되었고 현재의 CAN 통신은 baseband 만을 사용하기 때문에 증가되는 데이터 전송률의 수요를 만족하지 못한다. 이에 대한 해결책으로써, baseband 에서 확장하여 passband 를 사용하게 되면 더 많은 대역폭을 사용할 수 있으며, 시스템에 적합한 변조방식을 사용함으로써 데이터 전송률을 크게 향상시킬 수 있다. 그러나, 현재 passband 를 이용한 CAN 통신에 대한 연구는 거의 전무한 실정이며, 고속 CAN 통신을 위한 passband 를 사용하기 위해서는 각 주파수 대역에서의 채널 특성을 알아야 한다. 이러한 채널 특성을 알기 위한 채널 특성 측정을 대신해 채널을 모델링할 수 있다면, 채널 특성을 파악하는데 소요되는 시간과 노력을 크게 줄일 수 있을 것이다. 본 논문에서는 PLC 분야와 VDSL 분야에서 사용되고 있는 채널 모델링과 유사한 모델링 기법에 기반하여 CAN 시스템 고유의 bus 구조를 고려한 채널모델링을 제안한다. 또한, 채널 모델링 결과는 실험 결과와의 비교를 통해 정확도를 검증하였다. 최종적으로, 채널 모델링 결과를 이용하여 시스템 상의 다양한 조건 에서의 임펄스 응답과 시스템 최대 용량을 분석하였다.

핵심어 : Controller area network (CAN), 채널 모델링, AWG 24 꼬임 전선, 전송 행렬, 채널 용량.